IOP Publishing Nanotechnology
Nanotechnology 32 (2021) 142004 (28pp) https://doi.org/10.1088/1361-6528/abcf6c

Topical Review

Recent developments in the synthesis of chemically modified nanomaterials for use in dielectric and electronics applications

Bhausaheb V Tawade[1], Ikeoluwa E Apata[1], Maninderjeet Singh[2], Priyanka Das[3], Nihar Pradhan[3], Abdullah M Al-Enizi[4], Alamgir Karim[2] and Dharmaraj Raghavan[1]

[1] Department of Chemistry, Howard University, Washington DC, United States of America
[2] Department of Chemical and Biomolecular Engineering, University of Houston, Houston, TX 77204, United States of America
[3] Department of Chemistry, Physics and Atmospheric Science, Jackson State University, Jackson, MS-39217, United States of America
[4] Department of Chemistry, King Saud University, Riyadh 11451, Saudi Arabia

E-mail: draghavan@howard.edu

Received 14 August 2020, revised 25 September 2020
Accepted for publication 30 November 2020
Published 15 January 2021

Abstract

Polymer nanocomposites (PNC) have attracted enormous scientific and technological interest due to their applications in energy storage, electronics, biosensing, drug delivery, cosmetics and packaging industry. Nanomaterials (platelet, fibers, spheroids, whiskers, rods) dispersed in different types of polymer matrices constitute such PNC. The degree of dispersion of the inorganic nanomaterials in the polymer matrix, as well as the structured arrangement of the nanomaterials, are some of the key factors influencing the overall performance of the nanocomposite. To this end, the surface functionalization of the nanomaterials determines its state of dispersion within the polymer matrix. For energy storage and electronics, these nanomaterials are usually chosen for their dielectric properties for enhancing the performance of device applications. Although several reviews on surface modification of nanomaterials have been reported, a review on the surface functionalization of nanomaterials as it pertains to polymer dielectrics is currently lacking. This review summarizes the recent developments in the surface modification of important metal oxide dielectric nanomaterials including Silicon dioxide (SiO_2), titanium dioxide (TiO_2), barium titanate ($BaTiO_3$), and aluminum oxide (Al_2O_3) by chemical agents such as silanes, phosphonic acids, and dopamine. We report the impact of chemical modification of the nanomaterial on the dielectric performance (dielectric constant, breakdown strength, and energy density) of the nanocomposite. Aside from bringing novice and experts up to speed in the area of polymer dielectric nanocomposites, this review will serve as an intellectual resource in the selection of appropriate chemical agents for functionalizing nanomaterials for use in specific polymer matrix so as to potentially tune the final performance of nanocomposite.

Keywords: nanocomposites, dielectrics, nanomaterials surface modification, electronics

(Some figures may appear in colour only in the online journal)

Introduction

Consumer electronic devices [1, 2], smart and wearable electronics [3, 4], aerospace parts [5], telecommunications equipment [6, 7], the military industry [8], and the automobile industry [9, 10] require high-performance capacitors and other energy-storage devices. To meet the demand for capacitors in the above applications, capacitors based on ceramic materials have attracted increasing attention [11, 12]. Among the various ceramic materials, $BaTiO_3$ nano-materials have drawn special attention due to their high dielectric constant (as high as 7000) [13], low dissipation, and impressive piezoelectric properties [14, 15]. By tuning the morphology (e.g. nanoparticles, nanorods, nanowires, nanocubes), crystal type (e.g. cubic, tetragonal, orthorhombic), surface chemical composition, porosity, filler loading, and distributions, a range of dielectric composite material loaded with $BaTiO_3$ nanoparticles have been formulated [16–22].

On the other end of the spectrum, there are applications such as integrated circuit (IC) technology where dielectric materials having a low dielectric constant (κ) are particularly important [23, 24]. In the systems where close to a billion transistors have to be interconnected in an area below 1 cm^2, the low-κ materials are needed as inter-level dielectrics (ILD) to minimize the effects caused by reduced line widths and minimal line-to-line spacings. The ILD material can decrease relative capacitance delay, cross-talk noise, and power consumption [25] which is especially important for fast signal propagation in high-density devices and high-speed electronic circuits [26, 27]. In addition to their primary function of electrical isolation of circuit and device components, these materials also provide useful chemical and interfacial properties. For example, n-MOS and p-MOS transistors are commonly isolated with a dielectric in metal–oxide–semiconductor field-effect transistor (MOSFET) technology, by depositing SiO_2 in trench structures. The pictorial representation of MOSFET technology is shown in figure 1. A schematic of the MOSFET structure of field-effect transistor (FET) (figure 1(a)) and a modern CMOS transistor (figure 1(b)), consisting of the n-FET and p-FET pair, is shown in figure 1. The dopant profile in the source- and drain-region reflects modern planar CMOS technologies where an extended doped region is shown under the gate region in the channel. Additionally, a halo or pocket dopant implantation region is also shown in figure 1(b). These dopant regions have been incorporated in MOSFET to permit transistor channel scaling and increase the performance.

Several examples of low-κ dielectrics that include SiO_2, SiO_xN_y or SiN have been used as spacer dielectrics. Spacer dielectrics when used around the transistor *gate stack* promote isolation and implantation-profile control. The gate stack is defined here as the films and interfaces comprising the gate electrode, the underlying gate dielectric, and the channel region. The interface between the gate dielectric and the channel regions is particularly important in regard to device performance.

Organic thin-film transistor (OTFT) based on poly-(3-hexylthiophene) and aluminum oxide (Al_2O_3) have found utility as the gate dielectric [29] because Al_2O_3 has relatively moderate dielectric constant (between 7.5 and 9.5), is robust and it can be prepared on a variety of substrates with easy processing conditions. Furthermore, using Al_2O_3 as the top dielectric material, the transistor performance such as mobility and ON/OFF current ratio can be substantially enhanced. This is because the applied gate voltage in Al_2O_3 dielectric is much less compared to the SiO_2 dielectric [30].

Other nanocomposites including TiO_2 filled nanocomposites have been studied for use in capacitors and thin-film transistor (TFT) applications. Maliakal and coworker [31] formulated polystyrene (PS)/TiO_2 nanocomposite for use as a high-κ gate dielectric in flexible electronics applications (dielectric constant of composite ~8). Polystyrene/TiO_2 as TFTs exhibited carrier mobilities of ~0.2 $cm^2\ V^{-1}$.

A recent review article by He *et al* [32], highlights the benefits of using nanoparticles as additives to effectively control the crystal growth, film morphology, substrate wettability, and charge carrier mobilities, so as to promote the use of nanofilled organic semiconductor in TFT and other electronic device fabrication. Several review articles have been published to address the chemistry of low and high-κ materials [33–38]. And also there have been several review articles on polymer grafting of nanomaterials [39–41]. The review on surface functionalization of nanomaterials as it pertains to polymer dielectrics is currently lacking. Therefore, the aim of this review article is to provide a comprehensive overview of the efforts dedicated towards the synthesis of SiO_2, TiO_2, $BaTiO_3$, and Al_2O_3 nanomaterials and their surface modifications using traditional agents for use in electronics and dielectric applications.

Synthesis of nanomaterials

Nanomaterials are generally synthesized by two different approaches, (a) 'top-down' which is primarily a physical approach, (b) 'bottom-up' which is primarily a chemical approach. Table 1 compares the top-down and bottom-up approaches for the synthesis of nanomaterials.

For top-down approach, several physical methods have been reported including mechanical milling/ball milling, chemical etching, thermal ablation/laser ablation, explosion process, sputtering, etc. For bottom-up approach, several chemical methods have been reported such as chemical/electrochemical precipitation, vapor deposition, atomic/molecular condensation, solvothermal/hydrothermal, sol–gel process, microemulsion, spray pyrolysis, aerosol process, and biochemical reductions [42–47]. The attractive feature of bottom-up approach is that the nanomaterials of different shapes *viz.*, nanoparticles, nanorods and nanowires, can be synthesized using different reaction conditions and the use of different types of surfactants and/or solvents [33–37]. As an example, sol–gel method is primarily used to synthesize SiO_2 and Al_2O_3 nanomaterials while the hydrothermal method is primarily used to synthesize TiO_2, and $BaTiO_3$ nanomaterials. In this review, we initially describe the synthesis of SiO_2, TiO_2, $BaTiO_3$, Al_2O_3 nanomaterials followed by their surface functionalization.

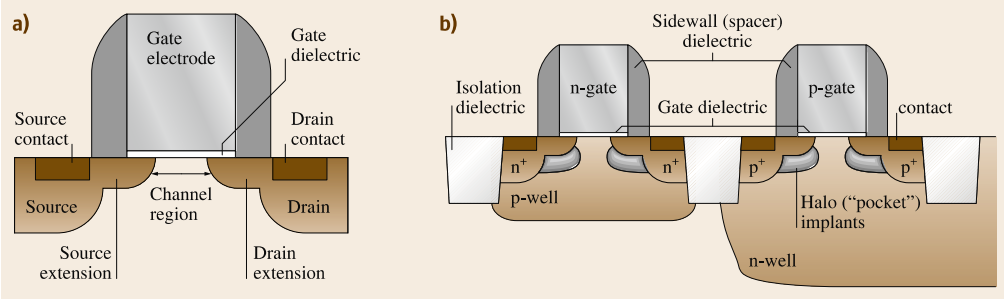

Figure 1. A pictorial representation of MOSFET technology. (a) A metal-oxide-semiconductor (MOS) field-effect transistor, and (b) a planar CMOS transistor structure [28].

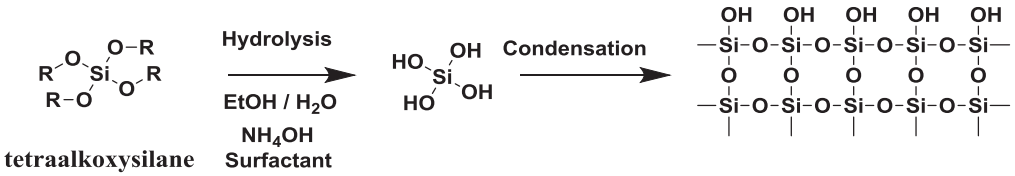

Scheme 1. General scheme for the synthesis of silica nanoparticle via sol–gel method.

Table 1. Top-down and bottom-up approaches for the synthesis of nanomaterials.

Top-down approach	Bottom-up approach
Scaling bulk materials to nanomaterials	Growing from atoms/molecules to nanomaterials
Synthesize in large amounts	Synthesize in small amounts (grams)
Nanomaterials synthesized can have defects and heterogeneous chemical composition	Nanomaterials synthesized have uniform size distribution with controlled size
Less ordered structures	More ordered structures
Easy and Cheap	Can be expensive
Generally, the physical technique is adopted	Generally, the chemical and/or biological technique is adopted
E.g. mechanical milling/ball milling, chemical etching, thermal ablation/laser ablation, explosion process, sputtering, etc	e.g. chemical/electrochemical precipitation, vapor deposition, atomic/molecular condensation, solvothermal/hydrothermal, sol–gel process, microemulsion, spray pyrolysis, aerosol process, and biochemical reductions

Synthesis of SiO_2 nanomaterials

Silica nanomaterials have been synthesized by various methods such as microemulsion, chemical vapor deposition, combustion, hydrothermal, plasma, and sol–gel techniques [48–53]. Among the various methods, sol–gel method is the most widely used method for the synthesis of SiO_2 nanoparticles and is based on simultaneous hydrolysis and condensation of the silicon alkoxides (scheme 1). Stober *et al* [49] used low-temperature synthesis to tune the nanoparticle characteristics by varying the composition of reactants, solvents, etc. A mixture of tetraethylorthosilicate (TEOS) or other silicates are reacted with water, in an alcohol and ammonia mixture to obtain particles whose final size (size range from 50 to 2000 nm) is influenced by the concentration of silicate, solvents, and additives used. The particle aggregation model seems to best describe the kinetics and mechanism of nanoparticles formation. Variations to Stöber method (such as the inclusion of surface-active agents and low pH) have resulted in the synthesis of mesoporous, hollow, and particles of different morphology as well as core–shell particles. Yamada and coworkers [54] synthesized four types of colloidal mesoporous silica particles with different particle diameters (ca. 20–80 nm) from tetraalkoxysilanes ($Si(OR)_4$, R = Me, Et, Pr, and Bu) by manipulating the hydrolysis rates of alkoxysilanes in a one-pot synthesis. Larger mesoporous particles can be synthesized by slowing the hydrolysis rate and allowing particle growth to dominate over nucleation. Alternatively, the size of nanoparticles can be manipulated using a sequential addition method of reacting TEOS to an aqueous alcohol mixture followed by the addition of NH_4OH [55].

Mesoporous silica particles of different morphology (nanospheres and nanorods) can be synthesized by using surfactant and solvent in varying concentrations [56]. The pore sizes and shapes of mesoporous nanoparticles were found to be highly dependent upon the characteristics of the surfactant (size, length, etc) and the micelle formation [57, 58]. For example, Vazquez *et al* [59] synthesized small

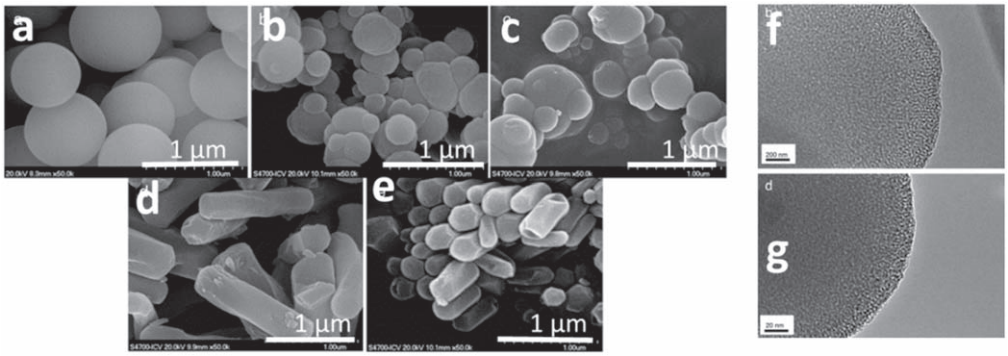

Figure 2. FESEM images of mesoporous silica particles with different concentration of surfactant (CTAB) (a) 0CTAB:45H_2O, (b) 0.1CTAB:45H_2O, (c) 0.3CTAB:45H_2O, (d) 0.3CTAB:600H_2O and (e) 0.3CTAB:1200H_2O; TEM images of mesoporous silica (f) and (g) [59].

Table 2. Synthesis of TiO_2 nanomaterial yielding various morphologies of varying aspect ratios.

Sr No.	Precursor	Surfactant/base/solvent/temp °C/[time]	Size and shape (phase)	References
1	Thiobenzoate Complex with Ti	Benzyl alcohol [30 min] Ethanol [10 min]	5–7 nm NPs (anatase)	[67]
2	$TiCl_4$	Ethanol 150°C [10 min]	10 nm NPs clustered into 500 nm aggregates (anatase)	[68]
3	Ti $(OCH(CH_3)_2)_4$	Oleic Acid/Toluene, 250 °C [20 h]	D = 3–6 nm L = 20–25 nm rod (anatase)	[69]
4	$Ti(OBu)_4$	Lauryl alcohol/Triethyl amine NH_4CO_3/Hexane 150 °C [24 h]	D = 4–20 nm L = 25–50 nm rod (anatase)	[70]

and large spherical as well as rod-shaped mesoporous silica nanoparticles by varying the cetyl trimethyl ammonium bromide (CTAB) (surfactant) to water ratio. The morphology of the particles can be tuned from spherical to rod by promoting particle growth in a certain direction. For example, an increase in the concentration of water changes the configuration of the surfactant micelles forming aggregates which encapsulate the silica precursor TEOS leading to decreasing the hydrolysis of TEOS and promoting the growth of the silica particle nonuniformly [60]. Additionally, the type of interactions between alkoxysilane and CTAB at the micelle/water interface could contribute to the changes in the growth of the particles in a certain direction. Figure 2 presents the FESEM and HRTEM images of mesoporous silica particles. The mesoporous silica particles are highly useful in nanocomposite dielectrics as 'degradation inhibitors' since they can sequester the electrical degradation products and slow the electrical aging especially under high-temperature conditions [61].

Synthesis of TiO_2 nanomaterials

Titanium oxide (TiO_2) nanomaterials have been synthesized using solvothermal/hydrothermal methods, sol–gel, templated-assisted approaches, electrochemical methods, chemical/physical vapor deposition, atomic layer deposition, pulsed laser deposition, pyrolysis, sonochemical, microwave-assisted, electrospinning methods, electrochemical etching methods, and photoelectrochemical etching methods, etc [62–64]. Among these methods, the hydrothermal method is preferred for the synthesis of TiO_2 nanoparticles because of the simple setup, facile operations, and desirable nanoparticle growth results etc. Like silica nanomaterial, TiO_2 nanomaterials can be synthesized by hydrolysis of the precursor titanium isopropoxide, $Ti[OCH(CH_3)_2]_4$ in isopropanol/water mixture with vigorous agitation followed by hydrothermal treatment [65, 66]. The hydrothermal treatment of the mixture at 95 °C for 24 h yields TiO_2 nanoparticles of defined shape. Hydrothermal treatment of TiO_2 precursor nanoparticles and acid washing can be used to introduce change to the crystallinity of the precursor nanoparticles from the anatase phase to a monoclinic phase, as well as the formation of TiO_2 nanosheets, and nanotubes. TiO_2 nanomaterials in anatase phase are generally obtained during solution-based or low-temperature vapor deposition preparations while high temperature deposition or annealing would usually yield rutile TiO_2 nanostructures. Brookite and TiO_2 (B) phases that are less common have also been obtained from solution-based growth systems [63]. Table 2 summarizes the precursors used and the variations adopted for the synthesis of

Table 3. Experimental conditions used for the synthesis of $BaTiO_3$ nanoparticles.

Precursors	Reaction conditions Temp and time	Size and shape	References
Hydrothermal method			
$Ba(OH)_2.8H_2O$ and $HClO_4$-TiO_2 or HCl–TiO_2	DI water, 160 °C, 3–24 h Ba/Ti ratio: 1.2	80–90 nm agglomerated nanoparticles	[75]
$Ba(OH)_2.8H_2O$, and $Ti(OC_4H_9)_4$	C_2H_5OH, ammonia solution, polyvinyl alcohol (PVA 1799), and NaOH, 200 °C for 48 h	68.8–75 nm nanoparticles	[76]
$BaCl_2.2H_2O$ and $TiCl_4$	DI Water, polyoxyethylene (20) sorbitan monooleate, KOH (pH = 13.5) 230 °C, for 0.5–2 h	77.8 ± 23.5 nm tetragonal nanoparticles	[77]
$Ba(OH)_2$ and TiO_2 particles	Ethanol, water, ammonia solution, 170 °C, 3 d	Nanowires, D = 50–200 nm and L = few to tens of μm	[78]
$Ba(NO_3)_2$ and $Ti(C_4H_9)_4$	DI water, NaOH, oleic acid, BuOH, 135 °C 18 h	22 nm cubic nanoparticles	[79]
Solvothermal method			
TiO_2 anatase, $Ba(OH)_2.8H_2O$	EtOH: H_2O (3:2); 90 °C–250 °C	30–200 nm, Nanotori, bulk or hollow nanospheres and nanocubes	[80]
$Ba(NO_3)_2$, $Ti(Bu)_4$	Oleic acid, BuOH 180 °C 18 h	16–30 nm for spheres	[81]
$Ba(OH)_2.8H_2O$ and titanium isopropoxide	Ethanol, and aq. NH_4OH solution, diethanolamine and triethanolamine 200 °C 48 h	80–100 nm Tetragonal nanoparticles	[82]
Sol–gel method			
$BaTi[OCH_2CH(CH_3)OCH_3]_6$	H_2O, n-butanol and 2-methoxypropanol, HCl 16 °C 15 h	6 nm nanoparticles	[83]
$Ba(OH)_2.8H_2O$, $Ti(OC_4H_9)_4$	polyvinyl pyrrolidone (PVP), ethylene glycol (EG), diethylene glycol (DEG), triethylene glycol (TEG), 45 °C–55 °C 2–10 h	2.8 and 5.1 nm nanoparticles	[84]
$(Ba(OCOCH_3)_2$ Titanium isopropoxide	Acetic acid, EtOH (62 °C), Masked Whatman anodisc membranes (200 nm pores)	Nanotubes with L = 50 μm D = 200 nm	[85]

TiO_2 nanorods and nanospheres through the hydrothermal method.

Synthesis of $BaTiO_3$ nanomaterials

Barium titanate ($BaTiO_3$) nanomaterials have received significant importance in recent years owing to their excellent dielectric, piezoelectric, and ferroelectric properties, flexibility in tuning its morphology, and broad use in energy storage, electronics, and devices applications [16, 42–44, 71–74]. Several methods have been reported for the synthesis of $BaTiO_3$ nanomaterial including hydro/solvothermal, template-assisted, molten salt, and sol–gel methods. These methods differ in chemistry and the type of organometallics used. Table 3 summarizes the methods and conditions employed to synthesize $BaTiO_3$ nanomaterial of various morphology. Among the various methods, the hydrothermal method has received significant attention because of the flexibility to control particle growth at low temperature, especially with the use of a single step processing protocol. Reaction below outlines the condensation of titanium oxide and barium hydroxide yielding barium titanate

$$Ba(OH)_2 + TiO_2 \xrightarrow{\Delta} BaTiO_3 + H_2O.$$

Synthesis of Al_2O_3 nanomaterials

Nano-sized alumina is a highly insulating, optically transparent, and chemically stable dielectric material with broad use in microelectronics. Several techniques have been employed for the synthesis of Al_2O_3 nanoparticles including ball milling [86], sol–gel [87], laser ablation [47], spray pyrolysis [88], hydrothermal [89, 90], atomic layer deposition, laser ablation [91, 92], co-precipitation, etc. The phase and morphology of synthesized alumina nanoparticles depend on the method of synthesis [93] which in turn dictates the dielectric properties of the nanomaterials [94, 95]. The sol–gel method is one of the widely used methods for the synthesis of Al_2O_3 nanoparticles. It involves the formation of oxide

Table 4. Surface energies and permittivity for various nanomaterials oxides [105].

Nanoparticles	Surface energy (J m^{-2})/permittivity	Nanoparticles	Surface energy (J m^{-2})/permittivity
α-Al_2O_3	2.6 ± 0.2/10.1 @ 1 MHz [106–108]	TiO_2 (anatase)	0.4 ± 0.1//∼31 @1 kHz [109]
γ-$A1_2O_3$	1.7 ± 0.1	Zeolitic silicas	0.09 ± 0.01/∼4 [110]
A1OOH (boehmite)	0.5 ± 0.1	SiO_2 (Amorphous, hydrated)	0.129 ± 0.008/3.8 @ 1 MHz [107] [111]
TiO_2 (rutile)	2.2 ± 0.2/114 @ 1 kHz [109]	SiO_2 (Amorphous, anhydrous)	0.259 ± 0.003 [111]
TiO_2 (brookite)	1.0 ± 0.2/93 @40 Hz [112]	$BaTiO_3$ [113]	1.01/1235 @ 1 kHz

network structure *via* the polycondensation reaction of precursors like aluminum nitrate and aluminum chloride when exposed to hydrous condition. Various factors like organic and inorganic additive precursors, solvents, stirring time, pH, water content and type of surfactants control the rate of hydrolysis and condensation during the sol–gel process [96]. For example, Mirjalili *et al* [46], synthesized nano α-alumina using sol–gel method with aluminum isopropoxide and aluminum nitrate as precursors along with 1, 3-benzene disulfonic acid disodium salt (SDBS) or sodium bis-2-ethylhexyl sulfosuccinate (Na(AOT)) as surfactant. SDBS facilitated the formation of well-defined spherical shaped amorphous α-alumina nanoparticles (20–30 nm) as opposed to (Na(AOT)). Adsorption of the SDBS surfactant on the surface of the intermediate boehmite nuclei phase hindered the aggregation of nanoparticles and restricted the grain growth of α-alumina nanoparticles [97].

A slight modification to the sol–gel method is the sol–gel auto combustion method where stable alpha phase alumina nanoparticles have been obtained at a by simultaneous decomposition of aluminum nitrate nonahydrate along with the use of urea or urea-glycine mixture as fuel [98]. Sharma *et al* concluded that the use of urea in high concentration as fuel produced crystalline phase nanoparticles whereas excessive use of glycine as fuel generated an amorphous phase of Al_2O_3 nanoparticles [99]. Various reports have concluded that processing temperature (calcination) is equally important in synthesizing thermodynamically stable alumina nanoparticles. The average crystallite size of alumina nanomaterial increases as the calcination temperature increases [98, 100–104].

Surface-functionalization of nanomaterials

Nanomaterials are highly reactive due to their relatively large surface area and small size. Additionally, due to the high surface energy of the inorganic nanofillers, the nanomaterials tend to aggregate, which is detrimental to the use of nanomaterial as additives in polymer matrix for dielectric and microelectronics application. The surface energy and dielectric permittivity values of the various oxides corresponding to their polymorphs are listed in table 4 [105].

For homogenous dispersion of nanofillers in the polymer matrix, the surface energy of the nanofillers generally has to be reduced. There are several approaches for decreasing the surface energy of nanomaterials and they include (a) introducing appropriate functional groups to the nanomaterial surface, (b) tethering monomers to the nanomaterial so as to promote polymerization under appropriate conditions (grafting from method), and (c) adding a linker group to the nanomaterial so that the linker could be used to covalently bond the terminal end of the grafted polymer chain to nanomaterial (grafting to method) [114]. The grafting to and grafting from methods are based on the use of harsh experimental conditions (water-free and oxygen-free), laborious, and use specialized equipment. Therefore, there is a need to evaluate less laborious and less equipment-intensive methods for the surface modification of nanofillers in the fabrication of polymer nanocomposites (PNC). Schmidt [115] initially proposed the concept of chemical modification of surface of nanoparticles along with the synthesis of silica nanoparticles based of sol–gel method. Thereafter, several surface modification approaches have been proposed including the use of organic or inorganic modifiers to functionalize nanomaterial [116]. Figure 3 shows the various chemical routes of modifying nanomaterials and the significance of chemical modification of nanomaterial as it relates to aggregated state as well as dispersed state [117–123].

Treatment of nanomaterial with hydrogen peroxide solution

Surface modification of nanomaterial with H_2O_2 is one of the effective ways to hydroxylate $BaTiO_3$, Al_2O_3 or TiO_2 nanomaterials. Table 5 summarizes the dielectric properties of PNC loaded with peroxide modified nanomaterial. Any enhancement in the dielectric properties of nanocomposite could be attributed (i) to the increased orientation polarization because of the introduction of polar –OH groups on the nanomaterial surface and (ii) hydrogen bond formation between nanoparticles and the polymer matrix. Chang *et al* [124] demonstrated the utility of hydroxylated $BaTiO_3$ nanoparticles to form oleophilic layers by reacting with sodium oleate (SOA) (figure 4). The SOA-modified $BaTiO_3$ was found to be readily dispersible in several polymer casting organic solvents.

TEM analysis of sodium oleate (SOA) modified $BaTiO_3$ nanoparticles revealed that SOA prefers to bond to the highly hydroxylated $BaTiO_3$ surface to form a homogeneous coating layer that is about 2 nm in thickness whereas without H_2O_2

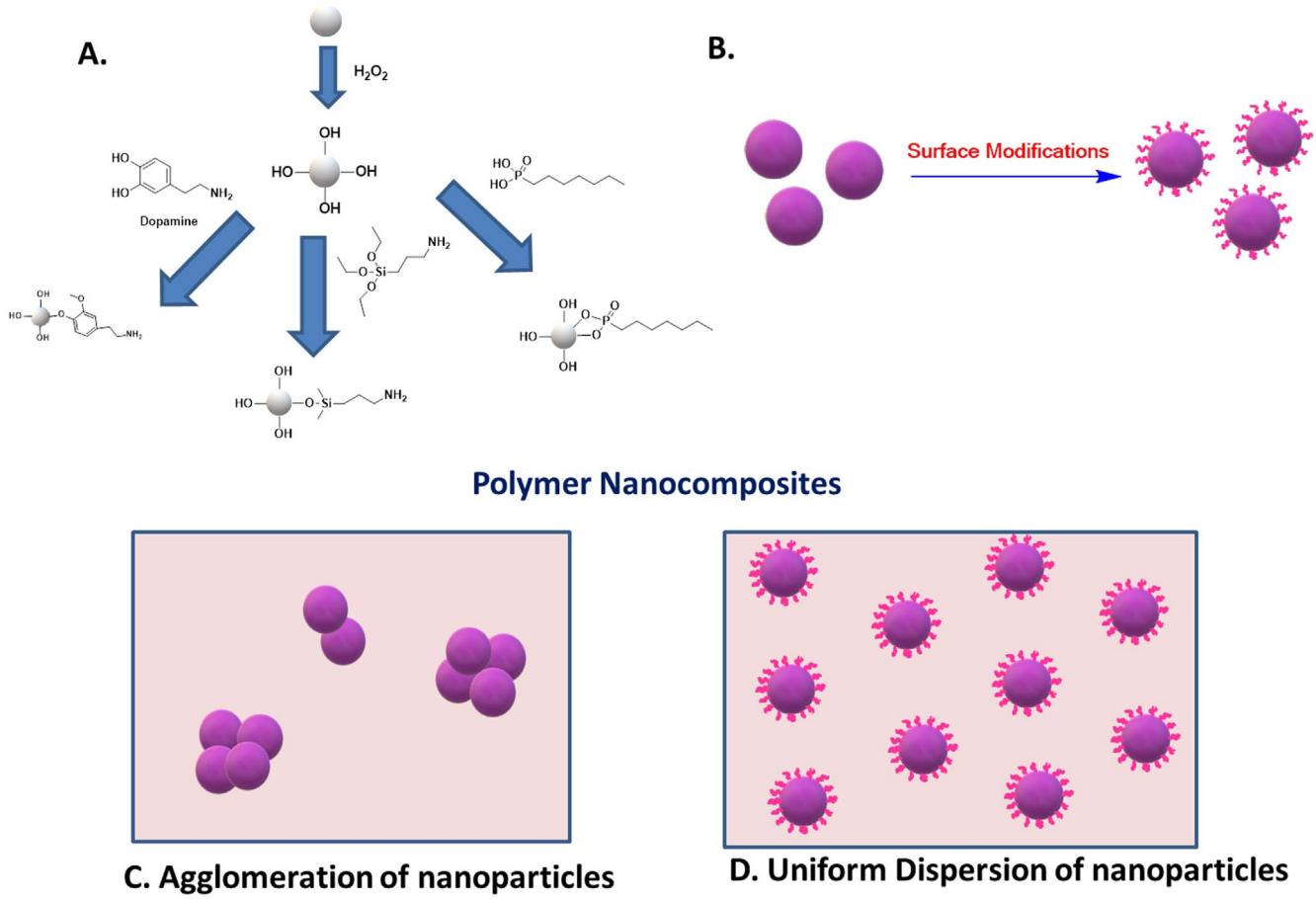

Figure 3. Pictorial representation of (A) common routes for surface modification of metal oxide nanoparticles; (B) surface modification reaction; (C) agglomeration of unmodified nanoparticles and (D) uniform dispersion of surface-modified nanoparticles in the polymer matrix.

Table 5. Summary of dielectric properties of polymer nanocomposites obtained with peroxide treated nanomaterials.

Filler	Mean Dia.	Volume fraction (%)	Matrix	Processing agent	ε_r		tan δ		E_b	
					B	A	B	A	B	A
$BaTiO_3$ (NP) [125]	70 nm	50 vol%	PEI	H_2O_2	33.87	52.78	NA	<0.03@1 kHz	NA	NA
$BaTiO_3$ (NP) [126]	85–100 nm	30 vol%	PVDF	H_2O_2	~80	~49	>0.075 @100 Hz	~0.075@100 Hz	NA	NA
Al_2O_3 (NP) [127]	100 nm	0.5 wt%	cured resin	H_2O_2	3.69	3.71	NA	0.007@1 kHz	64.82	68

Note. A is functionalized nanoparticle filled polymer nanocomposite and B is bare nanoparticle filled polymer nanocomposite.

pretreatment, only a little SOA binds to $BaTiO_3$ surface. Characteristic carbonyl peaks were noticed in the IR spectrum of SOA modified $BaTiO_3$ nanoparticles, unlike untreated nanoparticles. The amount of –OH groups formed on the nanoparticle surface increased with the duration of H_2O_2-treatment, reaching a maximum upon treatment for 4 h with 35% H_2O_2 aqueous solution. Using the Ghormley triiodide method [128], the decomposition of H_2O_2 on $BaTiO_3$ surface and the production of –OH groups can be followed. Figure 4(b) depicts the reaction mechanism for the production of –OH groups on the surface of the metal oxide via decomposition of H_2O_2. H_2O_2 upon decomposition form the hydroxyl radicals ($^{\cdot}OH$) as shown in equation (1). Then, the OH reacted with H_2O_2 to form the hydroperoxyl radical ($^{\cdot}OOH$) (equation (2)). The $^{\cdot}OOH$ radical then reacted with hydroxide radical to form water and oxygen (equation (3). Additionally, the $\cdot OOH$ can react with the oxide ions of the metal oxide ($O^{2-}_{(oxide)}$) to produce the hydroxyl group ($OH^{-}_{(oxide)}$) on the surfaces of nanoparticles. The conjugated base of $\cdot OOH$, the $O_2^{-}\cdot$ radical, produced from equation (4) can react with water to produce hydroxyl anions in aqueous solution ($OH^{-}_{(aq)}$) and $^{\cdot}OOH$ (equation (5)). Thus reactions (2)–(5) can self-propagate. Equation (6) shows the overall reaction of hydroxylation of nanomaterial surface.

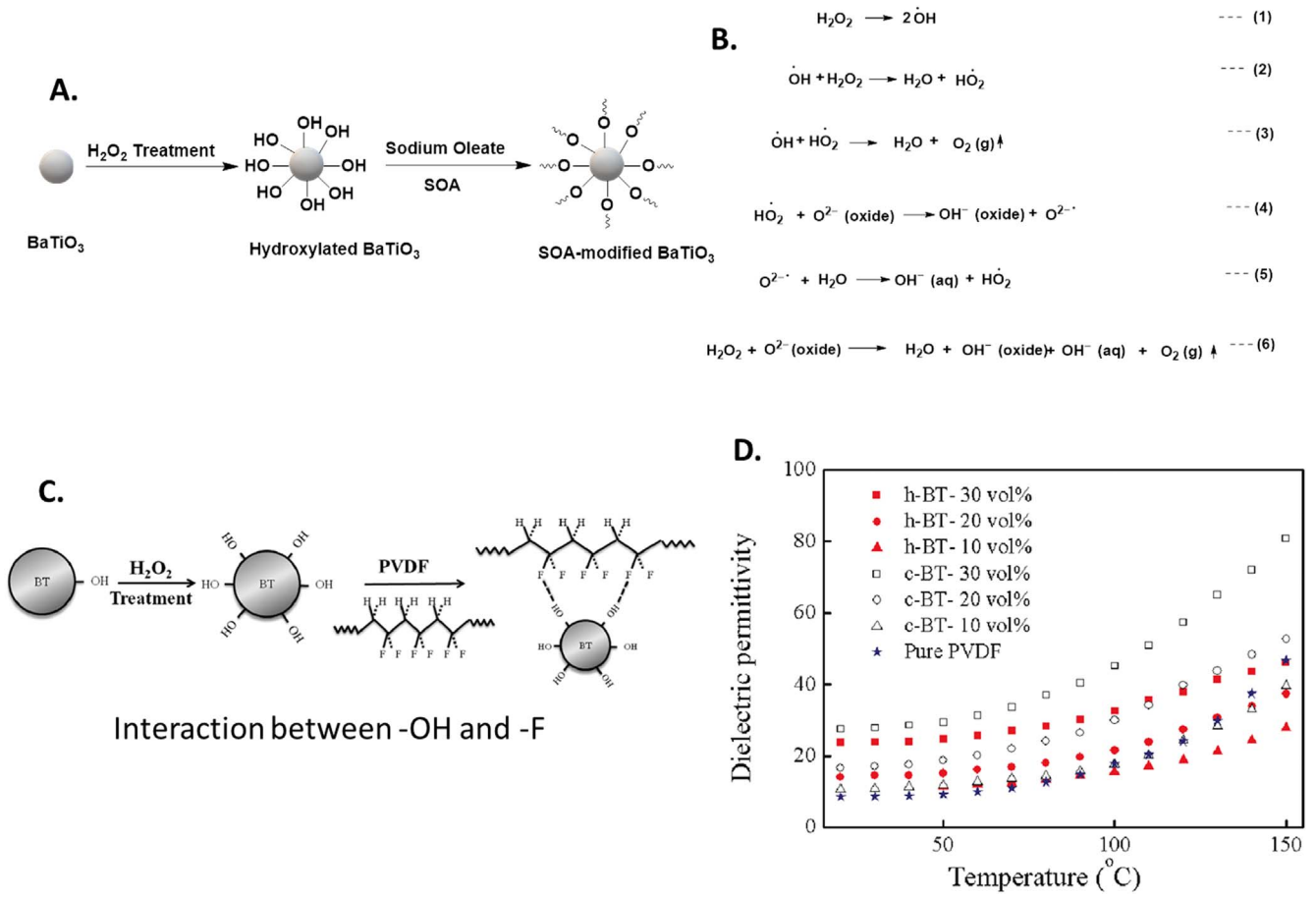

Figure 4. (A) The processes for hydroxylation and surface modification of $BaTiO_3$ nanoparticles; (B) reaction mechanism for surface hydroxylation; (C) schematic of the hydrogen bond in h-BT/PVDF nanocomposites; (D) temperature dependence of dielectric permittivity of nanocomposite obtained from hydroxylated $BaTiO_3$ (h-BT/PVDF) and unmodified $BaTiO_3$ (c-BT/PVDF) filled with various compositions at 100 Hz [126].

Choudhury [125] performed dielectric measurements of polyetherimide (PEI)/hydroxyl-functionalized $BaTiO_3$ nanocomposite films that were prepared by thermal imidization of the cast sample. The improved interaction between the hydroxyl-functionalized $BaTiO_3$ and the PEI matrix was found to improve the dispersion of the nanoparticles in the matrix and promote enhanced interfacial adhesion between polymer and nanoparticles. Additionally, the enhanced interaction between the –OH groups of functionalized $BaTiO_3$ and the imide groups of the PEI was found to reduce the void or pores formation in the nanocomposite films. The PEI nanocomposite with hydroxyl-functionalized $BaTiO_3$ nanoparticles showed an increased dielectric permittivity (52.78 at 1 kHz, 50 vol% $BaTiO_3$ loading) compared to the dielectric permittivity (33.87) of PEI/unmodified-$BaTiO_3$ composite. The dielectric loss was reduced (less than 0.03) when the loading of hydroxyl-functionalized $BaTiO_3$ was 50 vol%. Zhou and coworker [126], noted a similar benefit when hydroxylated $BaTiO_3$ nanoparticles were mixed with PVDF. For example, hydroxylated $BaTiO_3$/PVDF nanocomposite showed higher dielectric breakdown strength along with weaker dependence of dielectric permittivity as a function of temperature and frequency as compared to the unmodified- $BaTiO_3$/PVDF nanocomposites [126]. This is probably because of hydrogen bonding between hydroxylated nanoparticles and functional groups of PVDF backbone chain which promotes enhanced breakdown strength of nanocomposite. These observations are tabulated in table 5 and presented in figure 4. Similarly, an improved interaction between the hydroxyl group of hydroxylated-Al_2O_3 (h-Al_2O_3) and carboxyl groups on UV-cured resin resulted in an enhancement in the breakdown strength (64.82–68 kV mm^{-1}), and volume resistivity (5.47×10^{16}–10.2×10^{16} Ω cm^{-1}) of h-Al_2O_3 nanocomposite as compared to the untreated c-Al_2O_3 nanocomposite at 1 kHz with 0.5 wt% nanoparticle loading (table 5). The introduction of hydroxylated h-Al_2O_3 nanoparticles enhances the space charge suppression (3 kV mm^{-1} compared to 9 kV mm^{-1} of pure UV-cured resin) of nanocomposite [127].

There are examples where H_2O_2 modified SiO_2 can cause weakened interaction with substrate i.e. pentacene-based organic thin-film [129]. In this regard, it is important to understand the underlying chemical changes introduced on SiO_2 due to H_2O_2 treatment. In one of our earlier studies, we have observed a higher conversion of Si/Si–H to SiO_x/SiOH, and the growth of a thicker oxide layer on Si wafer upon long term exposure of silicon wafer to H_2O_2 and H_2SO_4 solution [130]. The formation of silanol groups (Si–OH) on the SiO_2 surface was based of the water contact angle measurement of the surface. The silanol groups on SiO_2 surface could promote

weakened interaction with pentacene, and reduction in field carrier mobility. However, Lin *et al* [129] contrary to the general observation [126, 127], reported an increase in the field-effect carrier mobility (μ) despite weak interaction between SiO_2 and pentacene. The increase in field-effect carrier mobility was attributed to the degradation of the *C–V* characteristics and reduction in the activation energy. Table 6 summarizes the transistor properties of surface-modified nanoparticles filled active layer.

Silane coupling agent treatment of nanomaterial

One of the common approaches adopted to modify the functionality of metal oxide nanoparticles is to react with silane coupling agents viz., alkoxysilanes, halosilanes. Yuan and co-workers [139] fabricated PTFE composite with modified SiO_2 nanoparticles (silanized by different compositions of silane agents (per-fluoro octyl triethoxysilane (PFOTES) and amino propyl triethoxy silane (APTES)). Interestingly, they observed that SiO_2 modified with 1.1 wt% PFOTES and 0.4 wt% APTES when added to PTFE resulted in an improvement in the dielectric properties ($\varepsilon r \sim 2.89$ (3% increase) and , $\tan\delta \sim 0.0007$ (A) (50% decrease) compared to the bare SiO_2 filled nanocomposite) [139]. Table 7 summarizes the dielectric properties of PNC loaded with silane-modified nanomaterial.

Instead of using amino-terminated short-chain silane agent to functionalize SiO_2, Bai *et al* [131], used a long alkyl chain silane agent (octadecyl trichlorosilane) to modify SiO_2 for gate dielectric purpose. A reduction in SiO_2 gate dielectric was observed resulting in significant improvement in the performance of OTFTs. The OTFT with octyl trichlorosilane (OTS) functionalized SiO_2 bilayer gate insulator configuration showed an increase in the field-effect mobility (6×10^{-4}–1.5×10^{-3} $cm^2\,V^{-1}\,s^{-1}$) and reduction in the threshold voltage (−9 V to –6 V) when compared to OTFT with bare SiO_2. The connectivity of the evaporated copper phthalocyanine (CuPc) thin-film on the OTS-treated SiO_2 was significantly improved due to the improved compatibility between the (aromatic and conjugated system CuPc) active layer and the long alkyl chain of silanized SiO_2.

Various silane coupling agents have been employed to modify SiO_2 in organic transistor (table 6). Dong *et al* [132] reported a five-fold increase in charge-carrier mobilities for OTFTs composed of P3HT films on trichloro (1H, 1H, 2H, 2H perfluorooctyl) silane (FTS) monolayers supported on SiO_2 dielectric substrates ($P3HT/FTS/SiO_2/Si$) when subjected to supercritical carbon dioxide ($scCO_2$) processing. Here again, it appears the improved compatibility between the active layer and the functionality present on SiO_2 surface resulted in improved OTFT performance.

Majewski *et al* [137], showed that long alkyl chain silane coupling agent can also be used to functionalize TiO_2 and can be used in conjunction with the solution-processed polymeric organic semiconductor poly(triarylamine) (PTAA) to improve the performance of organic field-effect transistors (OFETs). The mobility of the octadecyl trichlorosilane (ODTS) -treated $TiO_2/PTAA$ was found to be 3.5×10^{-3} compared to $<10^{-5}$ $cm^2\,V^{-1}\,s^{-1}$ for untreated $TiO_2/PTAA$ at threshold voltage of −0.28 V. The results indicated that the carrier mobility in the amorphous organic semiconductor is highly sensitive to the interfacial interaction between the active layer and the functionality introduced on TiO_2. The study also concluded that the nonpolar, alkyl chain of ODTS anchored on the oxide surface shields PTAA from most of the energetic disorder at the inorganic surface and also promotes enhancement in the carrier mobility.

The silanization of TiO_2 nanoparticles can be a two-step process. The first step is the activation of TiO_2, through the acid treatment commonly by the use of methane sulfonic acid to increase the surface concentration of hydroxyl groups present on the nanoparticle surface as per Cheng *et al* [154]. The second step is the surface modification of the acid-treated nanoparticles using silane coupling agent. Commonly, the use of modified nanoparticles with appropriate functional groups can promote the good dispersion of the nanoparticle in the polymer matrix. On the other hand, the bare nanoparticles tend to aggregate and serve as the defect site in the nanocomposite and distort the local electric field and lower the breakdown strength of the nanocomposite. The reason for the field distortions in aggregated system is the difference in the conductivity and permittivity between fillers and the polymer matrix under DC and AC conditions. In certain cases, despite the incompatibility between the functional group on the nanoparticle surface and the polymer, higher breakdown strength of nanocomposite has been reported [155]. This may be due to the dipoles at the particle/polymer interface affecting charge carrier transport and trapping. The polar groups could act as charge scattering centers, traps or play other roles in preventing the electrical treeing pathways from being readily formed [156].

Apart from the use of silanized nanoTiO_2 to increase the carrier mobility of OTFT, silanized nanoTiO_2 has been used to enhance the dielectric performance of PNC. For example, when 5% APTES modified nano-TiO_2 was used to fabricate PVDF-based nanocomposite, Khodaparst *et al* [145] reported a 74% increase in the permittivity at 0.1 Hz and a 30% increase in the permittivity at 1 kHz. The enhancement in the performance of the nanocomposite was primarily a result of the closeness of the surface tension values of PVDF (33.2 dynes cm^{-1}) and APTES (35 dynes cm^{-1}). Loading of aminopropyl trimethoxysilane treated TiO_2 nanofillers at 5 wt% to PE also resulted in the enhancement of the DC breakdown strength of polyethylene nanocomposite by 40% compared to untreated TiO_2 nanocomposite [155]. Similarly, loading of 1% 3-glycidoxypropyl-trimethoxy-silane (GPTMS) treated TiO_2 nanofiller to low-density polyethylene (LDPE) also yielded nanocomposite films that had breakdown strength of 265 kV mm^{-1} compared to 223 kV mm^{-1} for pure LDPE [144]. In these systems, it is conceivable that the terminal functional groups of the functionalized nanoparticles bend inward and hydrogen bonds with the hydroxyl group of the

Table 6. Summary of the transistor properties of the surface-modified nanoparticles incorporated in the active layer.

Filler	Mean Dia.	Volume F (%)	Matrix	Processing agent	Capacitance (nF cm^{-2})	E_b (MV cm^{-1})	V_T (V)	μ_{FET} cm^2 (V^{-1} s−1)
SiO_2 $^{(NP)}$ [129]	265 nm	NA	Pentacene- OTFTs	H_2O_2	1.0	NA	NA	0.05
SiO_2 $^{(NP)}$ [131]	230 nm	NA	CuPc-OTFT	OTS	NA	NA	−6	1.5×10^{-3}
SiO_2 $^{(NP)}$ [132]	300 nm	NA	OTFTs	OTS	NA	NA	∼−1.5	0.003
SiO_2 $^{(NP)}$ [132]	300 nm	NA	P3HT -OTFTs	FTS	NA	NA	∼−16	∼0.011
SiO_2 $^{(NT)}$ [133]	500 nm	NA	CNT-TFTs	OTS	∼35 @100 Hz	NA	2.1	91
SiO_2 $^{(NP)}$[134]	200 nm	NA	P3HT-OFET	APTMS	NA	NA	−1.9	$3.2 \times 10-^2$
SiO_2 $^{(NP)}$ [135]	300 nm	NA	NDI-C_{14}-OTFTs	ODPA	NA	NA	16	4.2×10^{-2}
SiO_2 $^{(NP)}$ [135]	300 nm	NA	NDI-C_{14}- OTFTs	NAPA	NA	NA	15	1.3×10^{-2}
SiO_2 $^{(NP)}$ [135]	300 nm	NA	NDI-C_{14}- OTFTs	TDPA	NA	NA	22	3.8×10^{-2}
SiO_2 $^{(NP)}$ [136]	100 nm	NA	PTCDI-C_{13}-TFTs	ODPA	NA	NA	NA	0.9
TiO_2 $^{(NP)}$ [137]	7.5 nm	NA	PTAA- OFETs	OTS	460 @ 800 Hz	NA	−0.28	0.0035
TiO_2 $^{(NP)}$ [137]	7.5 nm	NA	Pentacene—OFETs	OTS	465 @ 800 Hz	NA	−0.23	0.25
Al_2O_3 $^{(NP)}$ [138]	20-nm	7 wt%	Ph-BTBT-C_{10} TFTs	ODPA	∼14 @ 10 kHz	NA	−8.3	1.26 ± 0.06

Table 7. Dielectric properties of nanocomposites with silane-modified nanomaterials.

Filler	Mean Dia.	Volume F (%)	Matrix	Coupling agent (silane)	εr		tan δ		E_b (kV mm^{-1})	
					B	A	B	A	B	A
SiO_2 $^{(NP)}$ [140]	10–80 nm	5 wt%	Epoxy	APTES	4.53	4.70	0.0049	0.0076 @ 50 Hz	NA	NA
SiO_2@BCZT $^{(NF)}$ [141]	20 nm	1 vol%	PI	APTES	3.4	3.87 @ 1 Hz	NA	NA	318.9	358.81
SiO_2 $^{(NP)}$ [142]	7–20 nm	1 wt%	PSR	APTES	~4.8	~5.0 @ 800 KHz	NA	NA	NA	NA
SiO_2 $^{(NP)}$ [139]	9 μm	1 wt%	PTFE	PFOTES	2.82	2.886	0.0015	0.0007@ 10 GH	NA	NA
TiO_2 $^{(NP)}$ [143]	50 nm	17 wt%	SR	γ -MPTMS	NA	NA	~0.037	<0.02 @ 1000 Hz	~74	~92
TiO_2 $^{(NP)}$ [144]	30 nm	1 wt%	LDPE	GPTMS	NA	2.3 @ 1 kHz	NA	NA	223	265
TiO_2 $^{(NP)}$ [145]	15 nm	5 vol%	PVDF	APTES	8.75@ 1 kHz	12.5 @ 1 kHz	NA	NA	NA	NA
TiO_2 $^{(NP)}$ [142]	10 nm	1 wt%	PSR	APTES	~4.6	~4.8 @ 800 KHz	NA	NA	NA	NA
$BaTiO_3$ $^{(NP)}$ [119]	700 nm	40.0 vol%	PVDF	APTES	~41	~48	<0.05	<0.05@ 100 kHz	NA	NA
$BaTiO_3$ $^{(NP)}$ [146]	100 nm	20 vol%	PVDF	APTES	~18	~21 @ 100 Hz	NA	NA	71.64	E_o 116.24
$BaTiO_3$ $^{(NP)}$ [147]	1.1 μm	60 vol%	P (VDF–TrFE)	APTES	65	85	<0.2	<0.05@ 10 kHz	NA	NA
$BaTiO_3$ $^{(NP)}$ [146]	100 nm	20 vol%	PVDF	APTMS	~18	~20 @100 Hz	NA	NA	71.64	125.54
$BaTiO_3$ $^{(NP)}$ [148]	0.83 μm	8 wt%	Resin	APTES	NA	32	NA	0.014@ 10 Hz	NA	20.8
$BaTiO_3$ $^{(NP)}$ [149]	75 nm	60 vol%	Epoxy resin	GPTMS	~38	50 @10 kHz	NA	NA	NA	NA
$BaTiO_3$ $^{(NP)}$ [150]	0.1 μm	70 vol%	Epoxy resin	APTES	NA	49	NA	0.02@ 100 kHz	NA	NA
$BaTiO_3$ $^{(NP)}$ [151]	100 nm	50 vol%	EVM	APTES	4 @ 100 Hz	14@ 100 Hz	0.01	0.019 @ 100 Hz	~28	13
$BaTiO_3$ $^{(NP)}$ [152]	3 μm	40 wt%	BADCy	APTES	7.3 @20 MHz	9.3 @20 MHz	~0.0025	~0.0025 @20MHz	NA	NA
Al_2O_3 $^{(NP)}$ [108]	30 nm	5 wt%	Epoxy	APTES	4.65	~4.75	NA	~0.019 @100 Hz	28.5	30
Al_2O_3 $^{(NP)}$ [153]	2 μm	70 wt%	Epoxy	GPTMS	19.6	34.1	0.015	0.0075 @ 100 Hz	NA	NA
Al_2O_3 $^{(NP)}$ [153]	2 μm	70 wt%	Epoxy	APTES	19.6	21.2	0.015	0.006 @ 100 Hz	NA	NA

Note. A is functionalized nanoparticle filled polymer nanocomposite and B is bare nanoparticle filled polymer nanocomposite.

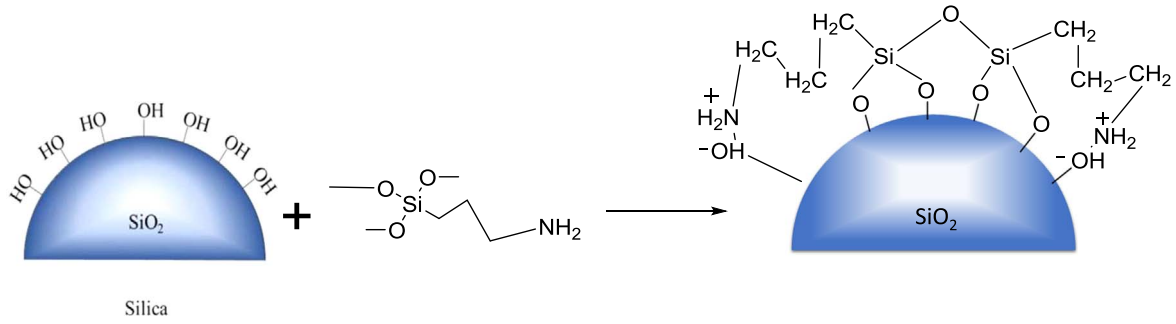

Figure 5. Hydrogen bonds formation between terminal amine of APTES and the hydroxyl group of the nanoparticles [157].

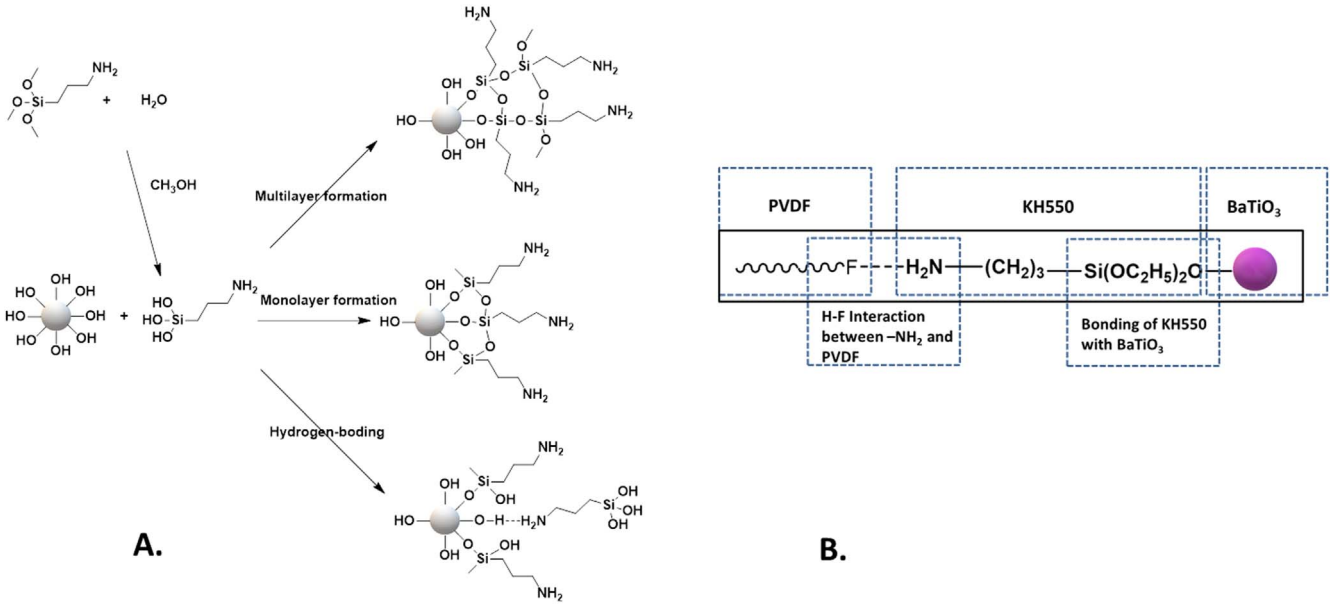

Figure 6. (A) Possible reaction between alkoxysilanes and hydroxylated nanoparticles; (B) schematic image of chemical reaction process of APTES with both surfaces of $BaTiO_3$ and PVDF. Rectangle with thick and black lines shows the bridge-linked action between $BaTiO_3$ and PVDF, which is benefit to the movement of polarized dipoles along the bridge.

nanoparticles thereby exposing the hydrocarbon backbone of the coupling agent for favorable interaction with LDPE matrix, hence the enhancement in the breakdown strength (figure 5).

Similar efforts to silanize $BaTiO_3$ nanoparticles have resulted in significant improvement in the dielectric performance of functionalized nanoparticles filled PNC. For example, Dang *et al* [119] noticed an improvement in the dispersion of nanoparticles when $BaTiO_3$ nanoparticles were modified with APTES and dispersed in polyvinylidene fluoride (PVDF) matrix. The study revealed that the nanocomposite of $BaTiO_3$ modified with 1 wt% of APTES has lesser pores and lesser voids. As indicated in figure 6, hydrogen bonding seems to play an important role in promoting the interaction between the functionality of the silanized nanoparticles and the polymer matrix and hence the improved dispersion and permittivity of the nanocomposite.

APTES modified $BaTiO_3$ nanoparticles have also been used as filler to enhance the dielectric properties of BPA cyanate ester and ethylene-vinyl acetate elastomer. For example, Chao *et al* [158] fabricated BPA cyanate ester nanocomposite with 40 wt% loading of APTES modified $BaTiO_3$ nanoparticles and it was found that APTES modified $BaTiO_3$/BADCy composites exhibited improved dielectric constant (9.3 at 20 MHz) and lower tanδ (0.0025 at 20 MHz) [152] compared to unmodified nanoparticle loaded nanocomposite.

Similarly, Xingyi and coworker [151], evaluated the effect of APTES functionalized $BaTiO_3$ nanoparticles on electrical, mechanical and thermal properties of ethylene-vinyl acetate elastomer (EVM) nanocomposites. It was found that the incorporation of surface modified $BaTiO_3$ nanoparticles into the EVM matrix not only increased the permittivity, thermal conductivity and the mechanical strength but also resulted in a comparatively lower dielectric loss tangent δ compared to pure EVM elastomer. The EVM nanocomposite exhibited relatively high dielectric strength and good ductility even at the 50 vol% nanoparticle loading [151].

When 3-glycidoxypropyl trimethoxysilane (GPTMS) functionalized nanoparticles were used along with epoxy resin as expected an improvement in the dispersion of $BaTiO_3$ nanoparticles in the epoxy resin was reported largely due to improved chemical compatibility [149]. As a part of the study, the silanization of $BaTiO_3$ nanoparticles with GPTMS was carried out in water, ethanol, and xylene to understand the importance of solvent selection in retaining the

functionality of functionalized nanoparticles. FT-nIR analysis revealed that the extent of terminal epoxy ring-opening was significantly higher when silanization was carried out in water and ethanol whereas it was minimum in xylene (i.e. maximum retention of epoxy groups on the surface of silanized $BaTiO_3$). The FT-nIR peaks attributed to epoxy ring were observed at 4522 and 5909 cm^{-1} for $BaTiO_3$ nanoparticles silanized using xylene, whereas the peaks corresponding to epoxy group were weaker for $BaTiO_3$ nanoparticles when silanized using ethanol. Furthermore, no peaks of epoxy ring were detected in the case of $BaTiO_3$ nanoparticles when silanization was conducted in water. The nanocomposite formulated with silanized $BaTiO_3$ nanoparticles (using xylene) exhibited a uniform composite structure with the highest dielectric constant ($\varepsilon r = 52$) (nearly 40% greater than that of unmodified $BaTiO_3$ filled nanocomposite) while the dielectric constant of nanocomposite where $BaTiO_3$ nanoparticles were silanized in ethanol and water was found to be 32 and 30, respectively. These results indicate that the selection of solvent for silanization plays a critical role in retaining the terminal end group of the functionalized nanoparticle. This has important implications in promoting the improved compatibility between resin and nanoparticles and enhancing the dielectric properties of the nanocomposite.

Apart from varying the end group functionality of the silane agent used in the functionalization of nanoparticles, there have been silanization studies performed wherein the nanoparticles were functionalized with silane agent of similar end group functionality but different hydrolyzable groups. For example, the silanization of hydroxylated $BaTiO_3$ (BT-OH) nanoparticles was carried out using 3-aminopropyltriethoxysilane (APTES) and 3-aminopropyltrimethoxysilane (APTMS) in toluene and ethanol [146]. The influence of the molecular structure of alkoxysilane attached to the surface of $BaTiO_3$ nanoparticles had a significant impact on the dielectric properties of PVDF-based nanocomposites. The breakdown strength of APTES modified $BaTiO_3$/PVDF nanocomposite ($E_b = 125.14$ MV m^{-1}) was higher than that of APTMS modified $BaTiO_3$/PVDF nanocomposite ($E_b = 116.24$ MV m^{-1}). The difference in the breakdown strength of the two systems can be attributed to the multilayer crosslinks formed between the adjacent silanized groups and/or the rate of hydrolysis of alkoxy groups that follow the trend MeO- > EtO- > t-BuO- and the ability to form a hydrogen bond between terminal functional group and the surface -OH group.

Apart from varying the end group functionality and the type of hydrolysable groups of the silane agent used in the functionalization of nanoparticles, there have been silanization studies performed wherein the nanoparticles were functionalized with silane agent of having mono-hydrolyzable and multi-hydrolyzable functional groups. It was found that silanes with multi-hydrolyzable functional groups are preferred for silanization of Al_2O_3 nanoparticles due to their better stability towards hydrolysis [159]. For example, (3-aminopropyl) dimethyl ethoxysilane, formed a self-assembled monolayer (SAMs) with Al_2O_3 nanoparticle which was sensitive to hydrolysis while the (3-aminopropyl) triethoxy silanized nanoparticle was significantly more robust due to the formation of a cross-linked multilayer siloxane linkage [160]. However, the cross-linked structure formed from the (3-aminopropyl) triethoxy silanized alumina nanoparticles was found to entrap the terminal amine groups in the multilayer and limit the availability of the amine group for further attachment [161]. On the other hand, APDMS (aminopropyl dimethoxy silane) formed a slightly thinner layer and afforded a larger fraction of functional groups from being available for further interaction with polymer. In other words, APDMS seems to the better candidate from the standpoint of robustness and availability of functional groups to enhance the interaction with polymer [162].

Yu and coworkers [108] have reported that surface modification of Al_2O_3 nanoparticles with γ-aminopropyl-triethoxysilane (APTES) can improve the dispersion of nanoparticles in epoxy matrix. A slight increase in the dielectric breakdown strength and dielectric constant was observed due to the functionalization of nanoparticles. The values for dielectric constant and breakdown strength were reported to be 4.65 and 28.5 kV mm^{-1} for 5 wt% epoxy/Al_2O_3 nanocomposite as opposed to 4.75 and 30 kV mm^{-1} for 5 wt% epoxy/silanized Al_2O_3 nanocomposite. Gong *et al* [163] modified core–shell structured Al@Al_2O_3 (where Al is the core and Al_2O_3 the shell) nanoparticle using γ-aminopropyl-triethoxysilane (APTES) and subsequently dispersed it in polyvinylidene fluoride (PVDF) matrix. An enhancement in the interfacial bond strength between the filler and the matrix was reported. For PVDF with 50 wt% of functionalized Al@Al_2O_3 the dielectric permittivity was reported to be 130 at 100 Hz frequency which was nearly 160% higher than that of PVDF with untreated Al@Al_2O_3 nanoparticle at the same filler content. This increase was attributed to the molecular bridge (hydrogen bonding) created by the silane coupler of the filler and the matrix.

Surface modification with phosphonic acid

Phosphonic acids and phosphate esters have been widely explored for the surface modification of hydroxylated surfaces [116]. Phosphonic acid shows superior reactivity with metal-oxide surfaces compared to conventional silane-based SAMs such as octadecyl trichlorosilane (OTS) and hexamethyldisilazane (HMDS) [164, 165]. Chemisorption can occur *via* the formation of covalent and hydrogen bonding between phosphonic acid and the hydroxyl groups on nanoparticle surfaces. Scheme 2 shows the mechanism of surface modification by phosphonic acid.

Several studies have used phosphonic acid-modified SiO_2 surfaces for gate dielectrics applications [135, 167]. For example, SiO_2 gate dielectric was modified by octadecyl phosphonic acid (ODPA), tetradecyl phosphonic acid (TDPA), and 6-naphthoxy-hexyl phosphonic acid (NAPA). The ODPA functionalized SiO_2 exhibited an increase in the electron mobility of N,N′-dialkyl-1,4,5,8-naphthalenediimides (NDI-Cn) (by nearly three orders of magnitude) compared to that of unmodified SiO_2. The modification of SiO_2

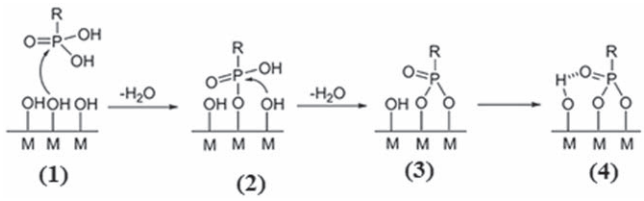

Scheme 2. Surface modification of metal oxides by phosphonic acid (1) hetero-condensation taking place between the phosphorus and a hydroxyl group on the surface, (2) repeating the hetero-condensation, (3) forming bidentate bound state, and (4) hydrogen bond formed between phosphoryl group and surface hydroxyl [166].

with ODPA resulted in an enhanced growth of NDI-C14 with fewer defects, the buildup of percolation pathways for electron accumulation and electron transport so as to prevent high charge density accumulation at the dielectric interface [135]. As shown in the AFM image (figure 7), NDI-C14 on bare SiO_2 exhibited poorly connected 3D grains with open grain boundaries that extend down the underlying substrate similar to that of NDI-C14 film on NAPA functionalized SiO_2. However, the ODPA/SiO_2 showed uniform coverage of NDI-C14 film with well-connected height circular grains associated with island growth mode, and these results support the observed enhancement in the field effect carrier mobility.

Similarly, the interaction between phosphonic acid-modified nanoparticles and the polymer matrix played a vital role in the dielectric performance of the nanocomposite. core–shell Ag/TiO_2 (Ag core and TiO_2 shell) nanoparticles modified with two phosphonic acids i.e. octyl phosphonic acid (OPA) and pentafluorobenzyl phosphonic acid (PFBPA), were dispersed in PTFE matrix [168]. The nanocomposites of PFBPA-modified core–shell Ag/TiO_2 (nanoparticles in PTFE ($\varepsilon r = 80$, $\tan\delta$ 0.4) exhibited better dielectric performance compared to OPA modified core–shell Ag/TiO_2 nanoparticles in PTFE ($\varepsilon r = 40$, $\tan\delta$ 0.5) at the same nanoparticle loading amount. This is because fluorinated structure of PFBPA promotes improved miscibility of TiO_2 nanoparticles in the PTFE matrix and promotes uniform dispersion of nanoparticles in the matrix [168]. Although OPA modified nanoparticles loaded PTFE showed inferior performance compared to PFBPA modified nanoparticles filled PTFE nanocomposite, the OPA functionalized nanoparticle filled PVDF nanocomposite fared better than octadecyl phosphonic acid (ODPA) modified nanoparticle filled PVDF nanocomposite. The dielectric constant of the PVDF nanocomposite with OPA modified nanofiller (148 at 1 kHz) was almost three times greater than that of nanocomposites with ODPA modified nano filler (58 at 1 kHz). The higher dielectric constant of the nanocomposite with OPA modified nanofiller was attributed to the enhanced dispersion of nanoparticles in PVDF matrix due to lesser steric hindrance and higher inorganic volume fraction of nanoparticles in the nanocomposite (figure 8) [169].

The type of phosphate ligand grafted on nanoparticles can equally influence the dielectric properties of phosphonic acid-modified nanoparticle filled nanocomposite [170]. Various organophosphate ligands namely phenyl phosphate (PP), aminophenyl phosphate (APP), nitrophenyl phosphate, (NPP), chlorophenyl phosphate (CPP), and aminoethyl phosphate (AEP) (figure 9) were used for the surface modification of TiO_2 nanoparticles [170]. It was observed that the nitrophenyl phosphate (NPP) modified TiO_2 nanoparticles filled nanocomposite exhibited significant improvement in breakdown strengths with reduced dielectric losses and leakage currents. This is because the NPP ligand has an electropositive phenyl ring with electron-withdrawing ($-NO_2$) groups which renders the molecule to be highly polar (as supported by Hammett correlation). The dipoles at the particle/polymer interface may affect charge carrier transport and trapping. The polar groups could act as charge scattering centers, traps or play other roles in preventing the electrical treeing pathways [170]. The maximum energy density of $\sim 3.2\ J{\cdot}cm^{-3}$ was observed for TiO_2-epoxy nanocomposites and $\sim 4.1\ J{\cdot}cm^{-3}$ for $BaTiO_3$-epoxy nanocomposites when 5 vol% of NPP modified nanoparticles was loaded [170] compared to $\sim 1.6\ J{\cdot}cm^{-3}$ and $\sim 2.9\ J{\cdot}cm^{-3}$ for unmodified TiO_2 filled epoxy nanocomposite and unmodified $BaTiO_3$-epoxy nanocomposites, respectively.

The selection of phosphate ligand for functionalizing nanoparticles for improving the functionalized nanoparticle's interaction with polymer matrix is also dependent on the type of the matrix. Kim *et al* [120] studied the effect of loading of different volume fractions of modified $BaTiO_3$ nanoparticles (with octylphosphonic acid (OPA), 2-[2-(2-methoxyethoxy) ethoxy]ethyl} phosphonic acid (PEGPA) and 2,3,4,5,6-pentafluorobenzyl phosphonic acid (PFPA)) on the dielectric properties of poly(vinylidene fluoride-*co*-hexafluoropropylene) (P(VDF-HFP)) and polycarbonate (PC) nanocomposite. An improved dispersion of PFPA modified nanoparticles was observed within the fluorinated polymer matrix and an increase in the relative permittivity of the resulting nanocomposite was observed compared to the nanocomposite with OPA modified nanoparticles (figure 10) [171]. For example, at 30 vol% nanoparticle loading, the permittivity of PFPA modified $BaTiO_3$ nanoparticle filled (P(VDF-HFP)), OPA modified $BaTiO_3$ nanoparticle filled (P(VDF-HFP)) and pure poly(VDF-HFP) was 20, 16 and 5 respectively. On the other hand, PEGPA modified $BaTiO_3$ nanoparticles was well dispersed in polycarbonate matrix as compared to the unmodified $BaTiO_3$ nanoparticles and enhanced dielectric performance ($\varepsilon r = 20 \pm 2$ at 1 kHz, $\tan\delta$ <0.01 at 1 MHz, breakdown strength $= 210 \pm 20\ kV\ mm^{-1}$, Energy density $= 3.9\ J\ cm^{-3}$) of 50% loaded PEGPA modified $BaTiO_3$ nanoparticle filled polycarbonate nanocomposite was noticed [172]. These results clearly highlight the importance of the selection of matrix-specific phosphonic acid for functionalizing nanomaterials so as to achieve potential improvement in the dielectric performance of nanocomposite.

The phosphonic acid-functionalized nanoparticle could induce a change in the crystal structure of the matrix which could impact the performance of the nanocomposite. When

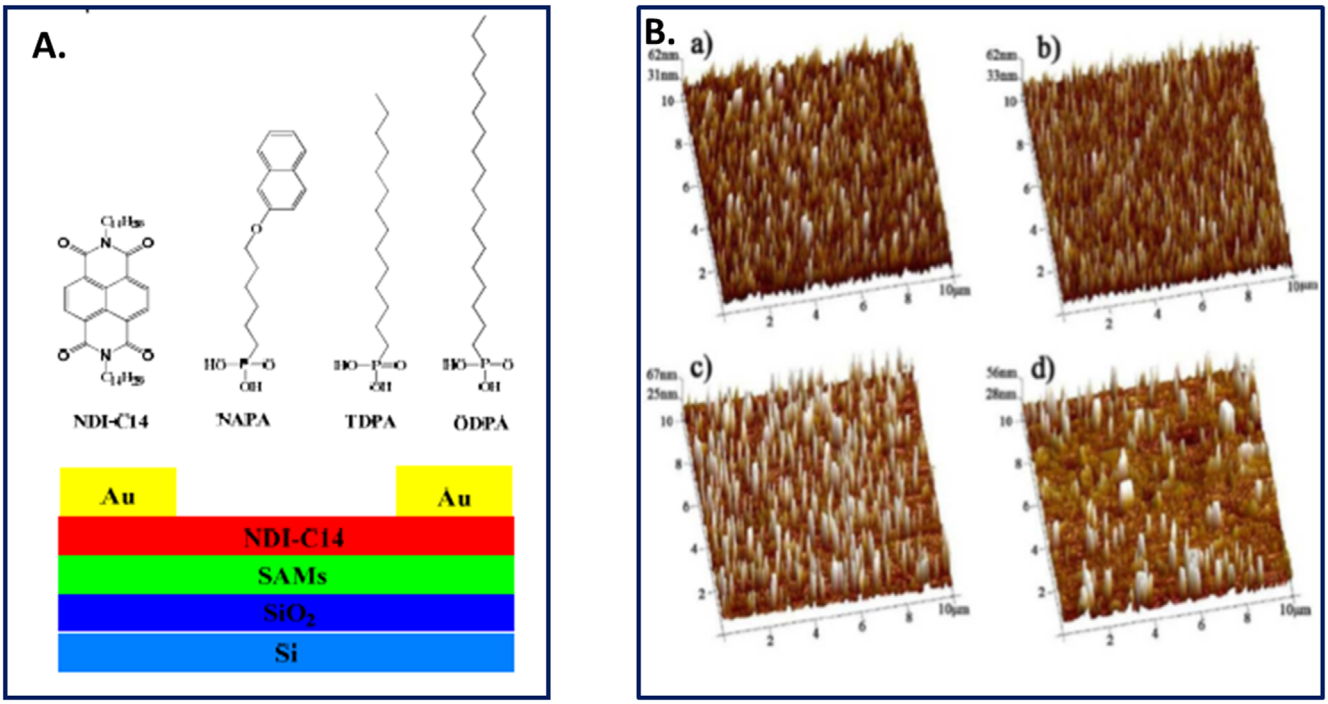

Figure 7. (A) Chemical structure of NDI-C14, SAMs molecules and schematic cross-section of TFTs (B) 3D AFM image of 80 nm NDI-C14 film on (a) ODPA/SiO_2, (b) TDPA/SiO_2 (c) NAPA-SiO_2 and (d) bare SiO_2 surface.

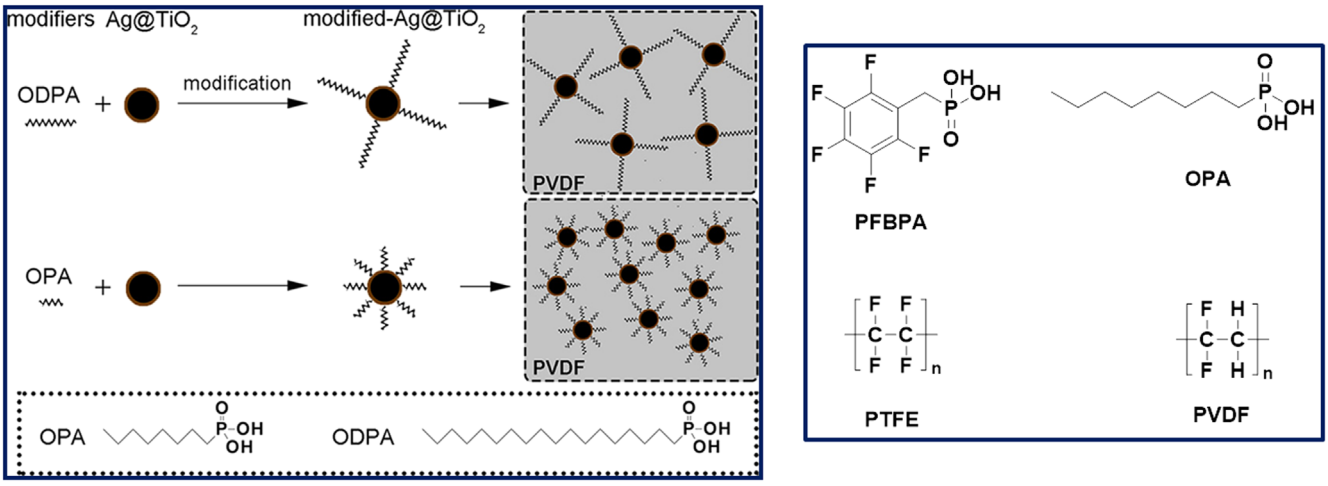

Figure 8. Modified nanoparticle filled polymer matrix. Chemical structures of pentafluorobenzyl phosphonic acid (PFBPA), polytetrafluoroethylene (PTFE), octyl phosphonic acid (OPA), and polyvinylidene fluoride (PVDF).

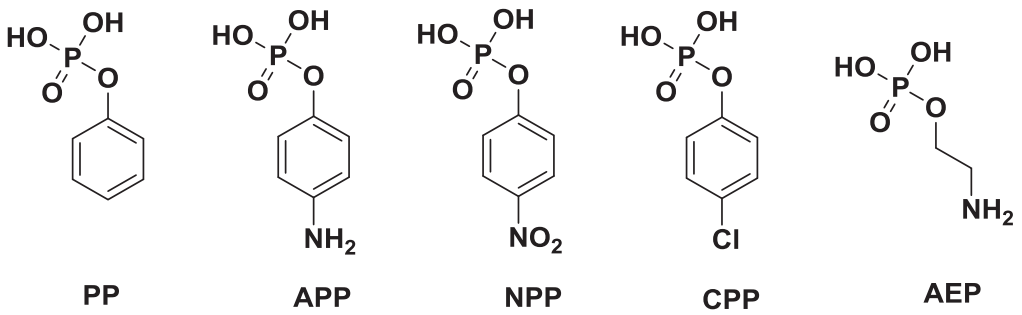

Figure 9. Molecular structures of organophosphate ligands: phenyl phosphate (PP), aminophenyl phosphate (APP), nitrophenyl phosphate (NPP), chlorophenyl phosphate (CPP), and aminoethyl phosphate (AEP) used to modify the surface of TiO_2 before dispersing in polymer.

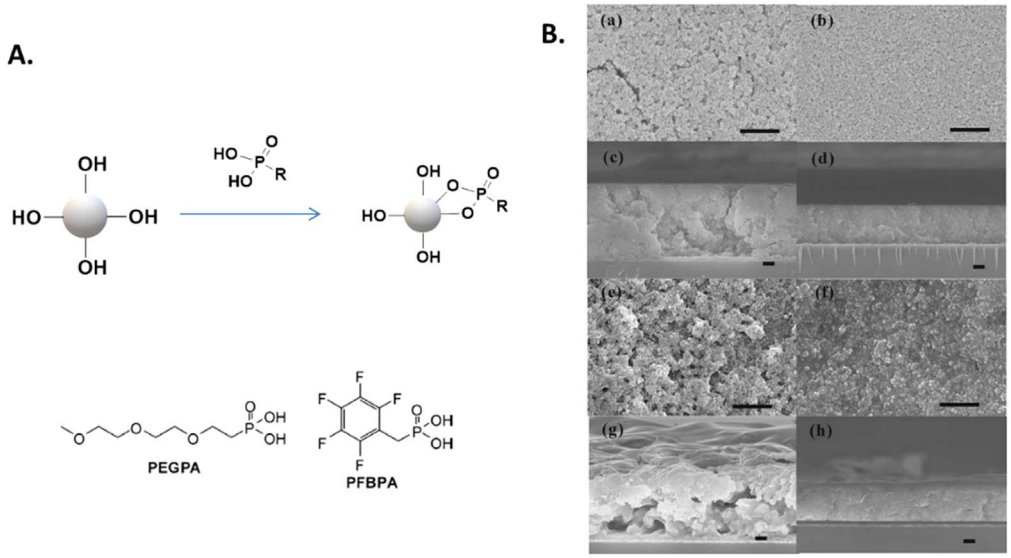

Figure 10. (A) The surface modification of $BaTiO_3$ with PEGPA and PFBPA; (B) surface and cross-sectional SEM images of spin-coated nanocomposite thin-films. (a), (c) BT/PC, (b), (d) PEGPA-BT/PC, (e), (g) BT/P(VDF-HFP), and (f), (h) PFBPA-BT/P(VDF-HFP). For unmodified BT, the nanocomposite contained 2 wt% of the BYK-w-9010 surfactant. All scale bars are 1 μm [172].

40 vol% tetradecylphosphonic acid (TDPA) modified $BaTiO_3$ nanoparticles were loaded to PVDF system, the nanocomposite exhibited a very high dielectric constant of 74.9 at 100 Hz and very low dielectric loss (0.05) compared to pure PVDF ~10.5 [173]. This is because the addition of TDPA-$BaTiO_3$ nanoparticles to PVDF causes a change of the crystal structure from the α-phase to β-phase. Moreover, in the applied electric field, the relaxation and orientation of dipoles are not restrained because of weak interaction between PVDF and TDPA functional group. This could possibly explain the enhanced dielectric constant in the PVDF nanocomposite compared to PVDF. Dielectric properties of phosphonic acid-functionalized nanomaterial filled PNC are tabulated in table 8.

The selection of the functional group on the nanoparticle could also have an impact on the thermal stability of the nanoparticles. A long-alkyl-terminated octadecyl phosphonic acid (ODPA) has been used as SAM for surface modification of α-Al_2O_3 for use on organic gate insulators (OGI). The results showed a remarkable decrease in the surface energy of OGI and enhanced molecular compatibility of the SAM layer with organic semiconductor (Ph-BTBT-C10) (table 6). The mobility of the Ph-BTBT-C10 TFTs was approximately doubled, from 0.56 ± 0.05 $cm^2\,V^{-1}{\cdot}s^{-1}$ to 1.26 ± 0.06 $cm^2\,V^{-1}{\cdot}s^{-1}$, after the surface treatment. The report also suggests that the surface treatment of α-Al_2O_3 with ODPA significantly decreased the threshold voltage from -21.2 V to -8.3 V by reducing the trap sites in the OGI and improving the interfacial properties [138].

Surface functionalization with Dopamine

One of the characteristics of dopamine modified nanoparticles is the versatility of dopamine to promote 'adhesion' with a variety of matrices [175]. Scheme 3 presents dopamine coordination to the metal oxide nanoparticles and the formation of an assembly of polydopamine thin-film on the surface of nanoparticles [176].

A systematic study of the functionalization of 1D nanomaterial with dopamine and its impact on the performance of nanocomposite was investigated using nanorods, nanorod arrays, and nanowires. When dopamine functionalized TiO_2 nanorod arrays were loaded at 6% to form P(VDF-HFP) nanocomposite, the nanocomposite had an ultrahigh energy density of 17.5 J cm^{-3} compared to 14.35 J cm^{-3} for pristine P(VDF-HFP) film at 509 kV mm^{-1}. Also at an electrical field as high as ~500 kV mm^{-1}, the charge-discharge efficiency of the nanocomposite was 86% compared to 76% in P(VDF-HFP). The results indicated that nanorod arrays along with dopamine modification can greatly improve the performance of dielectric composites [177]. Similarly, dopamine modified TiO_2 nanowires were loaded at 7.5 vol% to form P(VDF-HFP) nanocomposite and the dielectric constant of nanocomposite was 12.04 at 1 kHz compared to 5.01 for the neat P(VDF-HFP). The energy density of the nanocomposite was 1.35 J cm^{-3}, which was two times higher than that of the neat P(VDF-HFP) at field strength of 150 KV mm^{-1} [178]. Wang *et al* also established similarly the importance of dopamine modified TiO_2 nanowire for formulating high energy density P(VDF-HFP) nanocomposites (figure 11). The nanocomposite with 2.5 vol% dopamine modified TiO_2 nanowires exhibited an ultrahigh-energy storage density of 11.13 J cm^{-3} at 520 KV mm^{-1} whereas that of pure P(VDF-HFP) was 8.75 J cm^{-3} at 500 KV mm^{-1} [179]. All these results strongly suggest that one-dimensional (nanorods, nanowires, nanoarrays) with high aspect ratio along with surface modification by dopamine offer an opportunity to enhance the permittivity as well as the energy density of the nanocomposite. This is because one-dimensional nanofillers provide significant

Table 8. Summary of dielectric properties of polymer nanocomposites obtained with phosphonic acid surface modification of nanomaterials.

Fillers	Mean Dia.	Volume F (%)	Matrix	Processing agent	εr		tan δ		E_b (kV mm^{-1})		U (J cm^{-3})	
					B	A	B	A	B	A	B	A
Ag/TiO_2 $^{(NP)}$ [169]	12 mm	50 vol%	PVDF	ODPA	NA	58	NA	~0 .05 @ 1 kHz	NA	NA	NA	NA
Ag/TiO_2 $^{(NP)}$ [169]	12 mm	50 vol%	PVDF	OPA	NA	148	NA	~0 .05 @ 1 kHz	NA	NA	NA	NA
Ag/TiO_2 $^{(NP)}$ [168]	8–10 nm	70 vol%	PTFE	PFPBA	NA	~120	NA	~0.58 @ 100 Hz	NA	NA	NA	NA
Ag/TiO_2 $^{(NP)}$ [168]	8–10 nm	60 vol%	PTFE	OPA	NA	~40	NA	~0.5@100 Hz	NA	NA	NA	NA
TiO_2 $^{(NP)}$ [170]	32 nm	30 vol%	Epoxy	NPP	5.8	14.4	<0.024	<0.022 @ 10 kHz	NA	NA	1.6	~8 @ 355
$BaTiO_3$ $^{(NP)}$ [173]	70 nm	40 vol%	PVDF	TDPA	11	74.9	0.065	0.05 @ 100 Hz	NA	NA	NA	NA
$BaTiO_3$ $^{(NP)}$ [120]	30–50 nm	50 vol%	P(VDF-HFP)	PFBPA	12.5	35	~0.03	~0 .01 @ 1 kHz	~380	~220	NA	3.2 @ 164
$BaTiO_3$ $^{(NP)}$ [171]	20–50 nm	50 vol%	P(VDF-HFP)	PFBPA	5	~20	NA	0.04 @ 10 kHz	NA	~220	NA	3.2 $^{@}$ 64
$BaTiO_3$ $^{(NP)}$ [174]	<100 nm	50 vol%	P(VDF-HFP)	PFBPA	~5	57	NA	~0.08 @ 1 kHz	NA	90	NA	NA
$BaTiO_3$ $^{(NP)}$ [170]	30–50 nm	30 vol%	Epoxy	NNP	5.8	21.3	<0.024	<0.025 @ 10 kHz	NA	NA	NA	8.5 @ 300

Note. A is functionalized nanoparticle filled polymer nanocomposite and B is bare nanoparticle filled polymer nanocomposite.

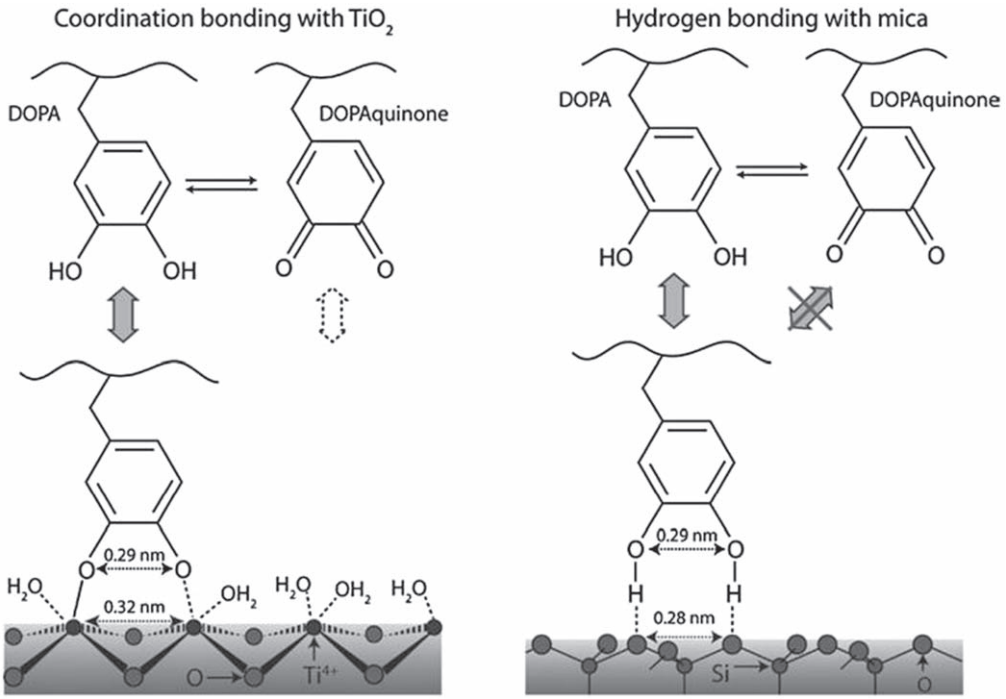

Scheme 3. Illustration of the proposed binding mechanism of DOPA to TiO_2 and mica surfaces.

scattering centers for charge dissipation and serve as obstacles for electrical treeing, while increasing the tortuosity of the breakdown path, resulting in higher energy density [177].

If indeed scattering centers are responsible for charge dissipation than 1D nanomaterial nanocomposites should show superior performance compared to 0D nanomaterial nanocomposite. A comparative dielectric study of PVDF nanocomposites based of dopamine modified TiO_2 nanowires and nanoparticles at 3 vol% was conducted. Assuming dopamine thickness is similar in both systems, the results indicate that the nanocomposites of nanowires (E_b = 380 MV m^{-1}) exhibited higher breakdown strength than the nanocomposites of nanoparticles (E_b = 220 MV m^{-1}), further confirming that the 1D nanomaterials provide more scattering centers compared to 0D nanomaterials. The dielectric properties of dopamine functionalized PNC are summarized in table 9.

Apart from the dimensionality of nanofiller playing an important role in the dielectric performance of nanocomposite, studies have also investigated the effect of dopamine functionalization of 0D material on the permittivity of the nanocomposite. Nano $BaTiO_3$@TiO_2 core@shell nanoparticles with gradient permittivity were coated with dopamine and used as filler to fabricate nanocomposite with P(VDF-HFP). The dielectric constant of the 20 vol% loaded $BaTiO_3$@TiO_2/P(VDF-HFP) nanocomposite was found to be 32.15 at 1 kHz which is significantly higher than that of pure P(VDF-HFP) (6.92) and exhibited low dielectric loss of 0.052. Additionally, the energy density of the nanocomposite was found to be 0.23 J cm^{-3} at 40 kV mm^{-1}, which was two times higher than that of pure P(VDF-HFP) [180] at lower field strength suggesting the role of dopamine and nanofiller in enhancing the dielectric performance of 0D nanomaterial filled nanocomposite.

Clearly, the above studies have demonstrated that dopamine functionalization of TiO_2 indeed improves the permittivity, breakdown strength and energy density of nanocomposite regardless of the dimensionality of the TiO_2 nanomaterial. Similar observations were also reported for dopamine functionalized $BaTiO_3$ nanocomposite. For example, when dopamine modified $BaTiO_3$ nanofibers were used as filler in poly(VDF-TrFE), an improvement in breakdown strength (200 kV mm^{-1}) and an enhancement in the dielectric constant (~30 for 10.8 vol% loading) of nanocomposite was observed compared to pure poly(VDF-TrFE) matrix ($E_b \sim 170$, $\varepsilon r = 13$) [117] Similarly, when dopamine modified $BaTiO_3$ nanowires were used as filler in P(VDF-CTFE), the nanocomposite exhibited enhanced energy density of 8.4 J cm^{-3} at a relatively low electric field of 2800 kV cm^{-1} compared to pure P(VDF-CTFE) (5.4 J cm^{-3} at 3600 kV cm^{-1}). The dopamine modified $BaTiO_3$ nanowires/nanofibers contributed to the enhancement in the dielectric properties of the nanocomposite. At 3 vol% loading of dopamine modified nanowires of whiskers, a 36% improvement (3000 kV cm^{-1}) in breakdown strength of P(VDF-CTFE) was observed compared to that of unmodified nanowires at similar % of nanowires of whiskers loading (2200 kV cm^{-1}) [184]. Nie and coworker [183], used dopamine-functionalized $BaTiO_3$ whiskers along with P(VDF-HFP (5% vol) and observed discharged energy of 9.0 J cm^{-3} which was nearly twice that of pure P(VDF-HFP)) [183]. Regardless of whether the nanomaterial was nanowire/nanofiber/whisker, the dopamine modified $BaTiO_3$ nanomaterial contributed to the enhancement in the dielectric properties of the PNC.

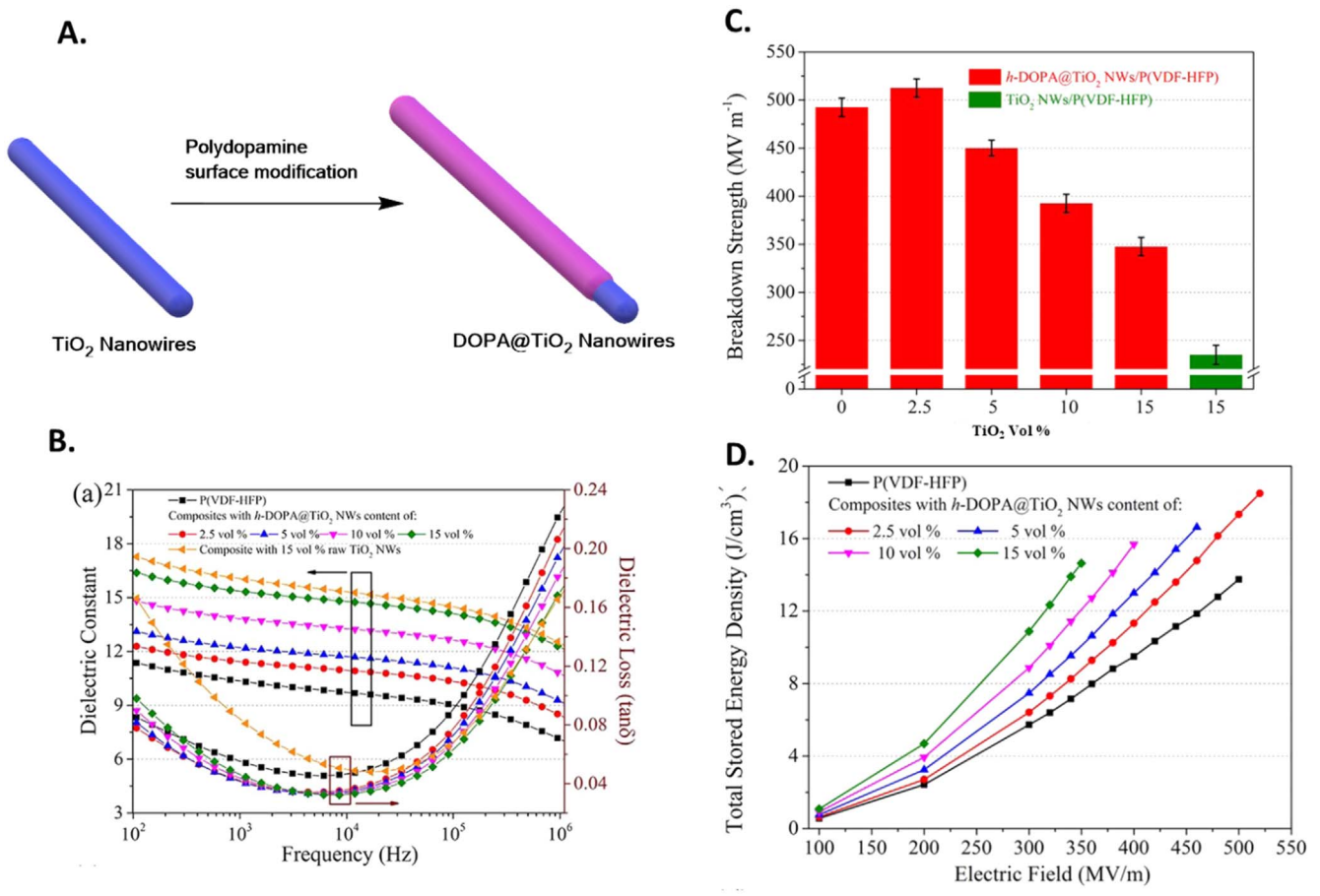

Figure 11. (A) Dopamine surface modification of TiO_2 nanowires into DOPA@TiO_2 NWs; (B) the dielectric constant and dielectric loss (tan δ) as a function of frequency at room temperature for *h*-DOPA@ TiO_2 NWs/P(VDF-HFP) nanocomposites. (C) Breakdown strength of the P(VDF-HFP)-based nanocomposites with different volume fractions of *h*-DOPA@ TiO_2 NWs and 15 vol. % raw TiO_2 NWs. (D) Discharged energy densities of *h*-DOPA@ TiO_2 NWs/P(VDF-HFP) nanocomposites with different volume fractions under varied applied fields [179]. Copyright permission received.

The significant enhancement in the energy density of the dopamine functionalized nanomaterial filled nanocomposite was attributed to the (i) phase change of the polymer near the interface induced by the $BaTiO_3$ nanomaterial and (ii) the improved dispersion of nanomaterial in the polymer matrix a result of improved H-bonding between OH group and NH_2 group of dopamine functionalized nanomaterial and the polymer matrix. Additionally, the polydopamine shells formed on the surface of the $BaTiO_3$ nanofibers can serve as the buffer layer in lowering the electric field concentration inside the polymer matrix, thereby preventing electrical treeing [117].

To understand the role of dopamine in influencing the polymorphs of polymer at the interface of the nanocomposite, Li *et al* [192] used dopamine modified $BaTiO_3$ nanowires/PVDF composite films. Clear phase transition of PVDF from α-phase to β-phase was noticed and it seems to originate from polydopamine interaction with PVDF matrix (figure 12). Furthermore, x-ray diffraction, Fourier transform infrared, and electric displacement-electric field (D-E) measurements revealed that nanocomposites of dopamine functionalized $BaTiO_3$ nanowires exhibited a higher fraction of β-phase content as compared to that of dopamine functionalized $BaTiO_3$ nanoparticles and unmodified $BaTiO_3$ nanowires. Since the β phase of PVDF shows improved piezo-, and ferro-electric properties among the various polymorphs of PVDF, the functionalization of nanomaterial by dopamine indeed is expected to improve the dielectric properties of the nanocomposite.

To establish the effect of polydopamine thickness of functionalized nanoparticles on the performance of $BaTiO_3$/PVDF nanocomposites Li and coworkers synthesized $BaTiO_3$ particles coated with different thicknesses of polydopamine layers of 5.5, 8 and 30 nm. Although the dielectric constant of composites filled with modified $BaTiO_3$ particles was found to be slightly lower than that of the composites filled with unmodified $BaTiO_3$ particles, significant suppression in the value of tanδ in the range of

Table 9. Summary of dielectric properties of polymer nanocomposites obtained with polydopamine surface modification of nanomaterials.

Filler	Mean Dia./length	Volume F (%)	Matrix	εr		tan δ		E_b (kV mm^{-1})		U (J cm^{-3})	
				B	A	B	A	B	A	B	A
TiO_2 $^{(NR)}$ [177]	100–200 nm/1.6 μm	6 vol%	P(VDF-HFP)	~13.1	18.2	~0.05	~0.05 @ 1 kHz	521	509	10.48	17.5 $^{@}$509
TiO_2 $^{(NW)}$ [178]	5 μm	7.5 vol%	P(VDF-HFP)	5.01	12.04	0.033	0.048 @ 1 kHz	~330	200	0.675	1.35 $^{@}$ 160
TiO_2 $^{(NW)}$ [179]	30 nm	2.5 vol%	P(VDF-HFP)	~9.5	10.5	~0.06	0.04 @ 10 kHz	<250	520	8.75	11.13 $^{@}$520
$BaTiO_3$@TiO_2 $^{(NP)}$ [180]	NA	20 vol%	P(VDF-HFP)	6.92	32.15	<0.052	0.052 @ 1 kHz	NA	NA	0.115	0.23 $^{@}$40
TiO_2 $^{(NP)}$ [181]	30 nm	30 phr	NBR	~13.5	16	~0.02	~0.02 @ 1 kHz	~62	65	NA	NA
$BaTiO_3$ $^{(NT)}$ [182]	150–250 nm/10 μm	10.8 vol%	PVDF	8.26	47.05	~0.04	0.04 @100 kHz	175	~200	NA	7.03 @ 330
$BaTiO_3$ $^{(NF)}$ [117]	200–250 nm/10 μm	10.8 vol%	(PVDF-TrFE)	14	27	~0.14	0.14 @ 100 kHz	170.9	204.8	NA	NA
$BaTiO_3$ $^{(WH)}$ [183]	NA	5 vol%	P(VDF-HFP)	~12	17.5	~0.05	0.05 @ 1 kHz	~275	~330	~5.5	9.02 @300
$BaTiO_3$ $^{(NW)}$ [184]	70 nm/10 μm	3 vol%	P(VDF-CTFE)	12	15.5	~0.06	0.06 @ 1 kHz	3700	3000	5.4	8.4 @ 2800
BCZT $^{(NP)}$ [185]	NA	25 vol%	epoxy resin	6.37	51	<0.2	0.25 @ 1000 Hz	NA	NA	NA	NA
$BaTiO_3$ $^{(NP)}$ [186]	NA	12 wt%	Epoxy resin	2.45	10.38	NA	NA	NA	NA	NA	NA
$BaTiO_3$ $^{(NP)}$ [187]	177 nm	40 wt%	PEN	3.5	10.7	0.03	0.07 @1000 Hz	NA	NA	NA	NA
Al_2O_3 $^{(NP)}$ [188]	300 nm	30 phr	NBR	10.95	11.43	~0.35	0.35 @ 1 kHz	NA	NA	NA	NA
Al_2O_3 $^{(NP)}$ [189]	300 nm	30 vol%	SR	2.59	4.06	0.001	0.003 @ 1 kHz	NA	NA	NA	NA
Al_2O_3 $^{(NP)}$ [190]	3 μm	25 wt%	PI	2.6	3.4	~0.08	0.02 @100 Hz	46.08	146.3	NA	NA
Al(Al@Al_2O_3) $^{(NP)}$ [191]	70 nm	50 wt%	PDVF	50	90.7	NA	0.24 @ 100 Hz	NA	NA	NA	NA

Note. A is functionalized nanoparticle filled polymer nanocomposite and B is bare nanoparticle filled polymer nanocomposite.

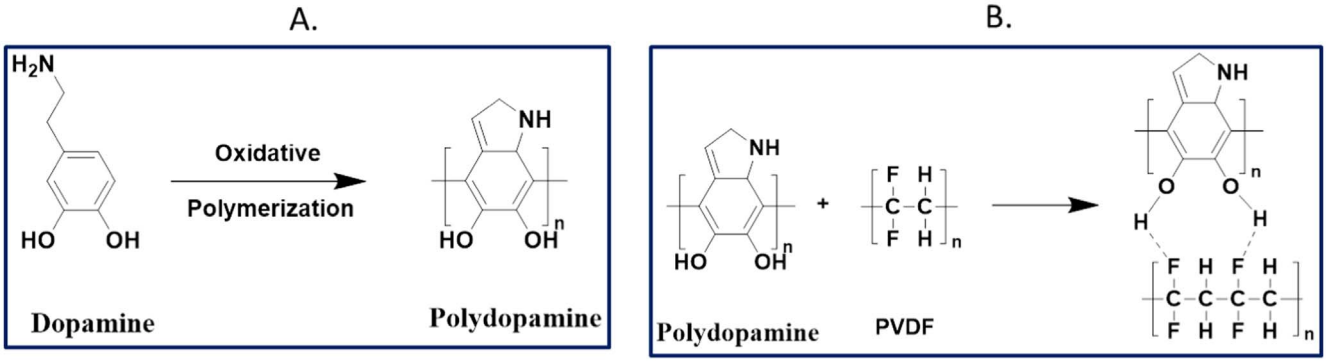

Figure 12. (a) The polymerization process of dopamine; (b) hydrogen bond formation between poly-dopamine and PVDF [192].

frequency lower than 10^3 Hz was observed. As the thickness of the polydopamine increases, the dielectric constant of the nanocomposite continues to decrease while an improvement in the dielectric loss was noticed [192].

Similarly, studies have indicated that the beneficial effect of dopamine modification of Al_2O_3 on lowering the interfacial tension between the nanoparticles and the polymer phases and preventing the agglomeration of the nanoparticles during processing [153, 163]. When 50 wt% of dopamine modified core@shell structured Al@Al_2O_3 nanoparticles was dispersed in PDVF, the dielectric permittivity increased to 90.7 at 100 Hz compared to 50 for unmodified Al@Al_2O_3/PVDF nanocomposite. The introduction of dopamine act as a molecular bridge between the matrix and the filler, which reduces the defects and voids at the interface and also helps with the polarization of the space charge under the action of the electric field [191]. Similarly, Ruan *et al* [188] synthesized surface-treated Al_2O_3 nanoparticles with mussel-inspired poly(dopamine) and dispersed the nanoparticles into nitrile rubber (NBR) and noticed an enhancement in the dielectric constant of Al_2O_3-PDA/NBR composite compared to composite filler with untreated Al_2O_3 nanoparticles loaded NBR composite.

Dopamine have also been used as a shell for core spherical alumina (PDA@Al_2O_3) along with hydroxyl grafted nano-sized boron nitride (nBN) as the outermost shell to generate a core-double shell bridge with 1,6-diisocyanatohexane (HDI) as the coupling agent. In the double core–shell structured nanomaterial filled polyimide nanocomposite, the polydopamine and nBN was reported to enhance the interfacial compatibility of the filler and polyimide. The reported breakdown strength was 68.5% higher than that of a pure PI and the dielectric constant was about 3.4 with 25 wt% f-BA as compared to 2.6 for the pure PI at 100 Hz [190]. These results indicate that the dopamine modification of nanomaterial contributed to the enhancement in the dielectric properties of the PNC irrespective of the type of nanomaterial.

Table 10 lists the advantages and disadvantages and suitability of the four surface modification methods for functionalizing nanoparticles.

Summary

High-*k* dielectric constant nanomaterials are important for formulating high-performance capacitors for potential use in consumer electronic devices, smart and wearable electronics, telecommunications equipment, while low-*k* nanomaterials are relevant for IC technology. This review highlights the various strategies that can be used to synthesize high-*k* and low-*k* nanomaterials. For example, sol–gel is primarily used to synthesize SiO_2 and Al_2O_3 nanoparticles while hydrothermal approach is primarily used to synthesize TiO_2, and $BaTiO_3$ nanoparticles. By using surface-active agents and acidic pH, sol–gel method can be used to synthesize mesoporous, hollow SiO_2 nanomaterial of different morphology and the core–shell nanoparticles. Likewise, hydrothermal treatment of TiO_2 precursor and acid washing can be used to introduce changes to the crystallinity of the precursor nanoparticles, from anatase phase to a monoclinic phase, to form TiO_2 nanosheets, nanotubes, nanoparticles and nanorod structures [193]. Varied approaches to synthesize nanocubes, nanotori, nanowires, and nanorods of $BaTiO_3$ have been presented, ranging from using sol–gel to solvo-hydrothermal approaches.

As the synthesized nanomaterials have high surface energies, they tend to aggregate strongly. An approach to improve the chemical compatibility of nanomaterial with polymer matrix is the treatment with peroxide, silane agent, phosphonic acid and/or dopamine. The peroxide treatment results in the formation of –OH groups (as outlined by the mechanism) which reached a maximum, upon treatment for 4 h with 35% H_2O_2 aqueous solution. Hydroxylated $BaTiO_3$ nanoparticles filled PVDF nanocomposites showed higher breakdown strength along with weaker dependence of dielectric permittivity as a function of temperature and frequency, as compared to the unmodified- $BaTiO_3$/PVDF nanocomposites. This is because of the hydrogen bonding interaction between hydroxylated nanoparticles and functional groups of PVDF backbone chain. Hydroxylated $BaTiO_3$ nanoparticles have also been silanized using 3-aminopropyltriethoxysilane (APTES) and 3-aminopropyltrimethoxysilane (APTMS) and

Table 10. Comparison of the advantages and the disadvantages of the surface modification methods.

Surface functionalization method	Advantages	Disadvantages
Hydrogen peroxide (H_2O_2)	Useful for the generation of hydroxyl groups on the surface	Reaction conditions are harsh and may cause decomposition of some nanomaterials
	It activates the surface of Nanomaterials for further reactions	One of the disadvantages of this technique is that the method produces only hydrophilic nanoparticle surfaces
Silane coupling agents	Variety of functionality anchored on the surface	Possibility of side reactions
	Useful for most of the metal oxide NPs	Such as multilayer formation, physical adsorption of silane coupling agent, etc
Phosphonic acids (PA)	PAs bind strongly to metal oxides and form robust monolayers on many different metal oxide materials	The limited reactivity of phosphonates towards SiO_2 causes weak physisorption and therefore can easily be washed off
	Modification of the functional R-groups on PAs allows us to control and tune the surface energy	The modification of nanoparticles with PAs can result in a side reaction—the formation of insoluble metal phosphonate salts
Dopamine (DA)	DA was used to cover the surface of nanoparticles to form a polydopamine layer which can be subsequently modified with molecules carrying nucleophilic groups	PDA works ideally for TiO_2, however, it has weaker attachments with substrates such as SiO_2, mica, nanoparticles, etc

the breakdown strength of APTES modified $BaTiO_3$ was found to be higher than that of APTMS modified $BaTiO_3$ filled nanocomposite, which was attributed to the multilayer cross-links formation between the adjacent silanized groups and/or the rate of hydrolysis of alkoxy groups which obeys the following trend MeO- > EtO- > t-BuO-. Solvents used for silanization of nanoparticles also influence the molecular structure of alkoxysilane grafted on nanoparticles and the dielectric properties of the overall nanocomposites. The dielectric permittivity of the nanocomposites filled with $BaTiO_3$ nanoparticles silanized in nonpolar solvent showed maximum permittivity, while nanocomposites filled with $BaTiO_3$ nanoparticles silanized in polar solvent showed minimum permittivity. Also, the number of hydrolyzable groups in the silane agent influences the molecular structure of alkoxysilane grafted on nanoparticles and the dielectric properties of the overall Al_2O_3 nanocomposites. From the standpoint of robustness and availability of functional groups, the silane agent with two hydrolyzable groups was found to be the best. Hydrogen bonding seems to play an important role in promoting the interaction between the functionality of the silanized nanoparticles and polymer matrix and thereby improving the dispersion and permittivity of the nanocomposite.

The type of phosphate ligand grafted on nanoparticles play an important role in influencing the dielectric properties of phosphonic acid modified nanoparticle filled nanocomposite. Various organophosphate ligands were used for the surface modification of TiO_2 nanoparticles. It was observed that the nitrophenyl phosphate (NPP) modified TiO_2 nanoparticles filled epoxy nanocomposite exhibited significant improvement in breakdown strengths with reduced dielectric losses and leakage currents. This is because the NPP ligand has electropositive phenyl ring with electron-withdrawing ($-NO_2$) groups which renders the molecule to be highly polar. The dipoles at the particle/polymer interface may affect charge carrier transport and trapping and could act as charge scattering centers, or play other roles in preventing the electrical treeing pathways from being readily formed.

The type of phosphate ligand grafted on nanoparticles is dictated by the type of polymer matrix used in the formulation of PNC. The improved dispersion of fluorinated phosphonic acid-modified nanoparticles was observed within the fluorinated polymer matrix, while the PEGPA-modified $BaTiO_3$ nanoparticles were well dispersed in polycarbonate matrix resulting in enhanced dielectric performance of the nanocomposites. These results clearly highlight the importance of the selection of matrix specific phosphonic acid agent for functionalizing nanomaterials so as to achieve optimum interaction and an improvement in the dielectric performance of nanocomposite.

Given the versatility of dopamine to promote 'adhesion' with a variety of the metal oxide nanoparticles and the ability of polydopamine thin-film to form on the surface of nanoparticles, it was noticed that one-dimensional nanomaterial (nanorods, nanowires) with high aspect ratio along with surface modification by dopamine offer an opportunity to enhance the permittivity as well as the energy density of the nanocomposite. This is because one-dimensional nanofillers provide significant scattering centers for charge dissipation and serve as obstacles for electrical treeing, while increasing the tortuosity of the breakdown path, resulting in higher energy density. Regardless of the type of nanomaterial or the dimensionality of the nanomaterial, the dopamine modified $BaTiO_3$ nanomaterial contributed to the enhancement in the dielectric properties of the PNC. The significant enhancement in the energy density of the dopamine functionalized nanomaterial filled nanocomposite was attributed to the (i) likely phase change of the polymer near the interface induced by the dopamine functionality of the nanomaterial and (ii) the improved dispersion of nanomaterial in the polymer matrix a

result of improved H-bonding between OH group and NH_2 group of dopamine functionalized nanomaterial and the polymer matrix. Also, the polydopamine shells formed on the surface of the nanomaterial can serve as the buffer layer in lowering the electric field concentration inside the polymer matrix, thereby preventing electrical treeing. Dopamine functionalization of nanomaterial of optimum thickness can be extremely useful in promoting significant enhancement in the energy density of the nanocomposite.

Recently the benefits of using nanoparticles as additives to effectively control the crystal growth, film morphology, substrate wettability, and charge carrier mobilities, so as to promote the use of nanofilled organic semiconductor in TFT and other electronics device fabrication was highlighted. Generally, a strong interaction between the SAM layer on the surface and the active layer could enhance the field carrier mobility and reduce the threshold voltage. For example, Bai *et al* used long alkyl chain silane coupling agent (octadecyl trichlorosilane) to modify hydroxylated SiO_2 gate dielectric. A reduction in SiO_2 gate dielectric was observed resulting in significant improvement in the performance of OTFTs which may be a result of the improved compatibility between the organic (aromatic and conjugated system copper phthalocyanine (CuPc)) active layer and the long alkyl chain of silanized SiO_2 nanoparticles. Similarly, long alkyl chain silane coupling agent was used to functionalize TiO_2 and was used in conjunction with the solution-processed polymeric organic semiconductor poly(triarylamine) (PTAA) to improve the performance of organic field-effect transistors (OFETs). The nonpolar, alkyl chain of ODTS anchored on the oxide surface shields PTAA from most of the energetic disorder at the inorganic surface and also promotes enhancement in the carrier mobility vis improved interfacial interaction. Similarly, the octadecyl phosphonic acid-functionalized SiO_2 exhibited an increase in the electron mobility of N,N′-dialkyl-1,4,5,8-naphthalenediimides (NDI-Cn) (by nearly three orders of magnitude) compared to that of unmodified SiO_2. The modification of SiO_2 with ODPA resulted in an enhanced growth of NDI-C14 with fewer defects, buildup of percolation pathways for electron accumulation and electron transport so as to prevent high charge density accumulation at the dielectric interface [135]. The selection of surface active-agent on the surface of nanoparticles/layer governs the dielectric properties of the nanocomposite as well as the performance of the bilayer as it relates to gate dielectrics.

Acknowledgments

The authors would like to thank the National Science Foundation (NSF) for financial support via Grant DMR-1901127. A K and A A-E also extend their sincere appreciation to the Researchers Supporting Project number (RSP-2020/55), King Saud University, Riyadh, Saudi Arabia for taking the time to review the manuscript.

ORCID iDs

Bhausaheb V Tawade https://orcid.org/0000-0001-7385-3643
Dharmaraj Raghavan https://orcid.org/0000-0002-7634-0656

References

[1] Hu C, Chen M, Li H, Zhang Z, Jiao Y and Shao H 2018 An accurate on-site calibration system for electronic voltage transformers using a standard capacitor *Meas. Sci. Technol.* **29** 055901
[2] Pourmousavian N, Kuo F-W, Siriburanon T, Babaie M and Staszewski R B 2018 A 0.5 V 1.6 mW 2.4 GHz Fractional-N all-digital pll for bluetooth LE with PVT-insensitive TDC using switched-capacitor doubler in 28 nm CMOS *IEEE J. Solid-State Circuits* **53** 2572–83
[3] Dubal D P, Chodankar N R, Kim D-H and Gomez-Romero P 2018 Towards flexible solid-state supercapacitors for smart and wearable electronics *Chem. Soc. Rev.* **47** 2065–129
[4] Li J, Jiang Q, Yuan N and Tang J 2018 A review on flexible and transparent energy storage system *Materials* **11** 2280
[5] Ho J S and Greenbaum S G 2018 Polymer capacitor dielectrics for high temperature applications *ACS Appl. Mater. Interfaces* **10** 29189–218
[6] Araga Y, Nagata M, Miura N, Ikeda H and Kikuchi K 2017 Superior decoupling capacitor for three-dimensional LSI with ultrawide communication bus *Japan. J. Appl. Phys.* **56** 04CC05
[7] Chen G, Peng H, Zeng R, Hu Y and Ni K 2018 A fundamental frequency sorting algorithm for capacitor voltage balance of modular multilevel converter with low-frequency carrier phase shift modulation *IEEE J. Emerg. Sel. Top. Power Electron.* **6** 1595–604
[8] Schunemann B, Schael U, Rauer G, Wickert M, Curath, R and Nau S 2014 Rapid recharging power supply for multiple-hit electrical armor *2014 17th International Symposium on Electromagnetic Launch Technology (La Jolla, CA, USA)* (IEEE) 1–6
[9] Rezzak D and Boudjerda N 2017 Management and control strategy of a hybrid energy source fuel cell/supercapacitor in electric vehicles *Int. Trans. Electr. Energy Syst.* **27** e2308
[10] Lee S and Kim J 2017 Implementation methodology of powertrain for series-hybrid military vehicles applications equipped with hybrid energy storage *Energy* **120** 229–40
[11] Gu L, Li T, Xu Y, Sun C, Yang Z, Zhu D and Chen D 2019 Effects of the particle size of $BaTiO_3$ fillers on fabrication and dielectric properties of $BaTiO_3$/Polymer/Al films for capacitor energy-storage application *Materials* **12** 439
[12] Zhou M, Liang R, Zhou Z and Dong X 2018 Novel $BaTiO_3$-based lead-free ceramic capacitors featuring high energy storage density, high power density, and excellent stability *J. Mater. Chem.* C **6** 8528–37
[13] Waugh M D 2010 Design solutions for DC bias in multilayer ceramic capacitors, Electronic Engineering Times Europe 8 (2010) 34–36.(accessed 3 July, 2020) (http://compel.ru/wordpress/wp-content/uploads/2014/01/Mark-D.-Waugh.pdf)
[14] Hassan M L, Ali A F, Salama A H and Abdel-Karim A M 2019 Novel cellulose nanofibers/barium titanate nanoparticles nanocomposites and their electrical properties *J. Phys. Org. Chem.* **32** e3897
[15] Zhang L, Wang Y, Xu M, Wei W and Deng Y 2019 Multiple interfacial modifications in poly(vinylidene fluoride)/Barium titanate nanocomposites via double-shell

architecture for significantly enhanced energy storage density *ACS Appl. Energy Mater.* **2** 5945–53
[16] Tao J, Cao S, Feng R and Deng Y 2020 High dielectric thin films based on barium titanate and cellulose nanofibrils *RSC Adv.* **10** 5758–65
[17] Fu J, Hou Y, Zheng M and Zhu M 2018 Comparative study of dielectric properties of the PVDF composites filled with spherical and rod-like $BaTiO_3$ derived by molten salt synthesis method *J. Mater. Sci.* **53** 7233–48
[18] Fu J, Hou Y, Zheng M, Wei Q, Zhu M and Yan H 2015 Improving dielectric properties of PVDF composites by employing surface modified strong polarized $BaTiO_3$ particles derived by Molten Salt method *ACS Appl. Mater. Interfaces* **7** 24480–91
[19] Hu P, Shen Y, Guan Y, Zhang X, Lin Y, Zhang Q and Nan C W 2014 Topological-structure modulated polymer nanocomposites exhibiting highly enhanced dielectric strength and energy density *Adv. Funct. Mater.* **24** 3172–8
[20] Zhang X, Jiang J, Shen Z, Dan Z, Li M, Lin Y, Nan C-W, Chen L and Shen Y 2018 Polymer nanocomposites with ultrahigh energy density and high discharge efficiency by modulating their nanostructures in three dimensions *Adv. Mater.* **30** 1707269
[21] Nawanil C, Makcharoen W, Khaosa-Ard K, Maluangnont T, Vittayakorn W, Isarakorn D and Vittayakorn N 2019 Electrical and dielectric properties of barium titanate—polydimethylsiloxane nanocomposite with 0-3 connectivity modified with carbon nanotube (CNT) *Integr. Ferroelectr.* **195** 46–57
[22] Jiang B, Iocozzia J, Zhao L, Zhang H, Harn Y-W, Chen Y and Lin Z 2019 Barium titanate at the nanoscale: controlled synthesis and dielectric and ferroelectric properties *Chem. Soc. Rev.* **48** 1194–228
[23] Ho P S, Leu J J and Lee W W 2003 *Low Dielectric Constant Materials for IC Applications* 9 (New York: Springer Science & Business Media)
[24] Maier G 2001 Low dielectric constant polymers for microelectronics *Prog. Polym. Sci.* **26** 3–65
[25] Croes K, Pantouvaki M, Carbonell L, Zhao L, Beyer G P and Tokei Z 2011 Comparison between intrinsic and integrated reliability properties of low-k materials *2011 Int. Reliab. Phys. Symp.* (Piscataway, NJ: IEEE) pp 2F.1–F.7
[26] Gupta T 2009 *Copper Interconnect Technology* (New York: Springer Science & Business Media)
[27] Laskowski Ł, Laskowska M, Vila N, Schabikowski M and Walcarius A 2019 Mesoporous silica-based materials for electronics-oriented applications *Molecules* **24** 2395
[28] Wallace R M 2017 Dielectric material for microelectronic *Springer Handbook of Electronic and Photonic Materials* ed S Kasap and P Capper (Cham, Switzerland: Springer) pp 615–44
[29] Fumagalli L, Natali D, Sampietro M, Peron E, Perissinotti F, Tallarida G and Ferrari S 2008 Al_2O_3 as gate dielectric for organic transistors: charge transport phenomena in poly-(3-hexylthiophene) based devices *Org. Electron.* **9** 198–208
[30] Yang W, Sun Q-Q, Geng Y, Chen L, Zhou P, Ding S-J and Zhang D W 2015 The integration of Sub-10 nm Gate Oxide on MoS_2 with ultra low leakage and enhanced mobility *Sci. Rep.* **5** 11921
[31] Maliakal A, Katz H, Cotts P M, Subramoney S and Mirau P 2005 Inorganic oxide core, polymer shell nanocomposite as a high K gate dielectric for flexible electronics applications *J. Am. Chem. Soc.* **127** 14655–62
[32] He Z, Zhang Z and Bi S 2020 Nanoparticles for organic electronics applications *Mater. Res. Express* **7** 012004
[33] Burda C, Chen X, Narayanan R and El-Sayed M A 2005 Chemistry and properties of nanocrystals of different shapes *Chem. Rev.* **105** 1025–102
[34] Nikam A V, Prasad B L V and Kulkarni A A 2018 Wet chemical synthesis of metal oxide nanoparticles: a review *CrystEngComm* **20** 5091–107
[35] Walton R I 2002 Subcritical solvothermal synthesis of condensed inorganic materials *Chem. Soc. Rev.* **31** 230–8
[36] Park J, Joo J, Kwon S G, Jang Y and Hyeon T 2007 Synthesis of monodisperse spherical nanocrystals *Angew. Chem., Int. Ed.* **46** 4630–60
[37] Hyeon T 2003 Chemical synthesis of magnetic nanoparticles *Chem. Commun.* **NA** 927–34
[38] Hulkoti N I and Taranath T C 2014 Biosynthesis of nanoparticles using microbes—a review *Colloids Surf.* B **121** 474–83
[39] Bouharras F E, Raihane M and Ameduri B 2020 Recent progress on core–shell structured $BaTiO_3$@polymer/fluorinated polymers nanocomposites for high energy storage: synthesis, dielectric properties and applications *Prog. Mater Sci.* **113** 100670
[40] Dang Z M, Yuan J K, Zha J W, Zhou T, Li S T and Hu G H 2012 Fundamentals, processes and applications of high-permittivity polymer-matrix composites *Prog. Mater Sci.* **57** 660–723
[41] Hanemann T and Szabó D V 2010 Polymer-nanoparticle composites: from synthesis to modern applications *Materials* **3** 3468–517
[42] Hong K, Lee T H, Suh J M, Yoon S-H and Jang H W 2019 Perspectives and challenges in multilayer ceramic capacitors for next generation electronics *J. Mater. Chem.* C **7** 9782–802
[43] Cai Q J, Gan Y, Chan-Park M B, Bin Yang H, Lu Z S, Li C M, Guo J and Dong Z L 2009 Solution-processable barium titanate and strontium titanate nanoparticle dielectrics for low-voltage organic thin-film transistors *Chem. Mater.* **21** 3153–61
[44] Maranganti R and Sharma P 2009 Atomistic determination of flexoelectric properties of crystalline dielectrics *Phys. Rev.* B **80** 054109
[45] Hayashi H, Noguchi T, Islam N M, Hakuta Y, Imai Y and Ueno N 2010 Hydrothermal synthesis of $BaTiO_3$ nanoparticles using a supercritical continuous flow reaction system *J. Cryst. Growth* **312** 1968–72
[46] Mirjalili F, Hasmaliza M and Abdullah L C 2010 Size-controlled synthesis of nano α-alumina particles through the sol–gel method *Ceram. Int.* **36** 1253–7
[47] Ismail R A, Zaidan S A and Kadhim R M 2017 Preparation and characterization of aluminum oxide nanoparticles by laser ablation in liquid as passivating and anti-reflection coating for silicon photodiodes *Appl. Nanosci.* **7** 477–87
[48] Kistler S S 1931 Coherent expanded aerogels and jellies *Nature* **127** 741
[49] Stöber W, Fink A and Bohn E 1968 Controlled growth of monodisperse silica spheres in the micron size range *J. Colloid Interface Sci.* **26** 62–9
[50] Vemury S, Pratsinis S E and Kibbey L 1997 Electrically controlled flame synthesis of nanophase TiO_2, SiO_2, and SnO_2 powders *J. Mater. Res.* **12** 1031–42
[51] Tani T, Watanabe N and Takatori K 2003 Emulsion combustion and flame spray synthesis of Zinc Oxide/Silica particles *J. Nanopart. Res.* **5** 39–46
[52] Yu Q, Wang P, Hu S, Hui J, Zhuang J and Wang X 2011 Hydrothermal synthesis of hollow silica spheres under acidic conditions *Langmuir* **27** 7185–91
[53] Choi S, Lee H and Park D-W 2016 Synthesis of silicon nanoparticles and nanowires by a nontransferred Arc plasma system *J. Nanomater.* **2016** 1–9
[54] Yamada H, Urata C, Aoyama Y, Osada S, Yamauchi Y and Kuroda K 2012 Preparation of colloidal mesoporous silica nanoparticles with different diameters and their unique

degradation behavior in static aqueous systems *Chem. Mater.* **24** 1462–71
[55] Rao K S, El-Hami K, Kodaki T, Matsushige K and Makino K 2005 A novel method for synthesis of silica nanoparticles *J. Colloid Interface Sci.* **289** 125–31
[56] Wu C, Wang Z, Quan G, Peng X, Pan X, Wang R, Xu Y, Li G and Wu C 2012 *In vitro* and *in vivo* evaluation of ordered mesoporous silica as a novel adsorbent in liquisolid formulation *Int. J. Nanomed.* **7** 199–209
[57] Castro Y, Molero E, Parente P, Duran A, Sanchez-Herencia A J and Ferrari B 2014 Electric field driven assembly of hybrid micelles for shaping of porous silica films *Adv. Appl. Ceram.* **113** 28–34
[58] Möller K, Kobler J and Bein T 2007 Colloidal suspensions of nanometer-sized mesoporous silica *Adv. Funct. Mater.* **17** 605–12
[59] Vazquez N I, Gonzalez Z, Ferrari B and Castro Y 2017 Synthesis of mesoporous silica nanoparticles by sol–gel as nanocontainer for future drug delivery applications *Bol. Soc. Esp. Ceram. Vidr.* **56** 139–45
[60] Lelong G, Bhattacharyya S, Kline S, Cacciaguerra T, Gonzalez M A and Saboungi M-L 2008 Effect of surfactant concentration on the morphology and texture of MCM-41 materials *J. Phys. Chem.* C **112** 10674–80
[61] Yang Y, Hu J and He J 2016 Mesoporous nano-silica serves as the degradation inhibitor in polymer dielectrics *Sci. Rep.* **6** 28749
[62] Lee K, Mazare A and Schmuki P 2014 One-dimensional titanium dioxide nanomaterials: nanotubes *Chem. Rev.* **114** 9385–454
[63] Wang X, Li Z, Shi J and Yu Y 2014 One-dimensional titanium dioxide nanomaterials: nanowires, nanorods, and nanobelts *Chem. Rev.* **114** 9346–84
[64] Fattakhova-Rohlfing D, Zaleska A and Bein T 2014 Three-dimensional titanium dioxide nanomaterials *Chem. Rev.* **114** 9487–558
[65] Wang C-C and Ying J Y 1999 Sol−gel synthesis and hydrothermal processing of anatase and rutile titania nanocrystals *Chem. Mater.* **11** 3113–20
[66] Vasilaki E, Kaliva M, Katsarakis N and Vamvakaki M 2017 Well-defined copolymers synthesized by RAFT polymerization as effective modifiers to enhance the photocatalytic performance of TiO_2 *Appl. Surf. Sci.* **399** 106–13
[67] Dar M I, Chandiran A K, Grätzel M, Nazeeruddin M K and Shivashankar S A 2014 Controlled synthesis of TiO_2 nanoparticles and nanospheres using a microwave assisted approach for their application in dye-sensitized solar cells *J. Mater. Chem.* A **2** 1662–7
[68] Wang X, Tian J, Fei C, Lv L, Wang Y and Cao G 2015 Rapid construction of TiO_2 aggregates using microwave assisted synthesis and its application for dye-sensitized solar cells *RSC Adv.* **5** 8622–9
[69] Kim C-S, Moon B K, Park J-H, Choi B-C and Seo H-J 2003 Solvothermal synthesis of nanocrystalline TiO_2 in toluene with surfactant *J. Cryst. Growth* **257** 309–15
[70] Li X-L, Peng Q, Yi J-X, Wang X and Li Y 2006 Near Monodisperse TiO_2 nanoparticles and nanorods *Chem.—Eur. J.* **12** 2383–91
[71] Liu J, Shen Z, Yao W, Zhao Y and Mukherjee A K 2010 Visible and infrared transparency in lead-free bulk $BaTiO_3$ and $SrTiO_3$ nanoceramics *Nanotechnology* **21** 075706
[72] Haertling G H 1999 Ferroelectric ceramics: history and technology *J. Am. Ceram. Soc.* **82** 797–818
[73] Kotecki D E *et al* 1999 (Ba,Sr)TiO_3 dielectrics for future stacked- capacitor DRAM *IBM J. Res. Dev.* **43** 367–82
[74] Preis W and Sitte W 2006 Electronic conductivity and chemical diffusion in n-conducting barium titanate ceramics at high temperatures *Solid State Ion.* **177** 3093–8
[75] Sasirekha N and Rajesh B 2008 Hydrothermal synthesis of barium titanate: effect of titania precursor and calcination temperature on phase transition *Ind. Eng. Chem. Res.* **47** 1868–75
[76] Chen H, Wang J, Yin X, Xing C, Li J, Qiao H and Shi F 2019 Hydrothermal synthesis of $BaTiO_3$ nanoparticles and role of PVA concentration in preparation *Mater. Res. Express* **6** 055028
[77] Wei Lu S, Lee B I, Lin Wang Z and Samuels W D 2000 Hydrothermal synthesis and structural characterization of $BaTiO_3$ nanocrystals *J. Cryst. Growth* **219** 269–76
[78] Joshi U A and Lee J S 2005 Template-free hydrothermal synthesis of single-crystalline barium titanate and strontium titanate nanowires *Small* **1** 1172–6
[79] Adireddy S, Lin C, Cao B, Zhou W and Caruntu G 2010 Solution-based growth of monodisperse cube-Like $BaTiO_3$ colloidal nanocrystals *Chem. Mater.* **22** 1946–8
[80] Bogicevic C, Thorner G, Karolak F, Haghi-Ashtiani P and Kiat J-M 2015 Morphogenesis mechanisms in the solvothermal synthesis of $BaTiO_3$ from titanate nanorods and nanotubes *Nanoscale* **7** 3594–603
[81] Caruntu D, Rostamzadeh T, Costanzo T, Salemizadeh Parizi S and Caruntu G 2015 Solvothermal synthesis and controlled self-assembly of monodisperse titanium-based perovskite colloidal nanocrystals *Nanoscale* **7** 12955–69
[82] Lee H-W, Moon S, Choi C-H and Kim D K 2012 Synthesis and size control of tetragonal barium titanate nanopowders by Facile Solvothermal method *J. Am. Ceram. Soc.* **95** 2429–34
[83] Brutchey R L and Morse D E 2006 Template-free, low-temperature synthesis of crystalline barium titanate nanoparticles under bio-inspired conditions *Angew. Chem., Int. Ed.* **45** 6564–6
[84] Hao Y, Wang X, Kim J and Li L 2014 Rapid formation of nanocrystalline $BaTiO_3$ and its highly stable sol *J. Am. Ceram. Soc.* **97** 3434–41
[85] Hernandez B A, Chang K-S, Fisher E R and Dorhout P K 2002 Sol−gel template synthesis and characterization of $BaTiO_3$ and $PbTiO_3$ nanotubes *Chem. Mater.* **14** 480–2
[86] Reid C B, Forrester J S, Goodshaw H J, Kisi E H and Suaning G J 2008 A study in the mechanical milling of alumina powder *Ceram. Int.* **34** 1551–6
[87] Mirjalili F, Hasmaliza M and Abdullah L C 2010 Size-controlled synthesis of nano a -alumina particles through the sol–gel method *Ceram. Int.* **36** 1253–7
[88] Kavitha R and Jayaram V 2006 Deposition and characterization of alumina films produced by combustion flame pyrolysis *Surf. Coat. Technol.* **201** 2491–9
[89] Yang J, Mei S and Ferreira J M F 2003 Hydrothermal synthesis of submicrometer α-alumina from seeded tetraethylammonium hydroxide-peptized aluminum hydroxide *J. Am. Ceram. Soc.* **86** 2055–8
[90] Sōmiya S and Roy R 2000 Hydrothermal synthesis of fine oxide powders *Bull. Mater. Sci.* **23** 453–60
[91] Ritala M and Leskela M 2002 Atomic layer deposition *Handbook of Thin Films Materials* (*Deposition and processing of thin films* 1) ed H S Nalwa 1 (Cambridge, MA: Academic Press) 103–59
[92] George S M, Ott A W and Klaus J W 1996 Surface chemistry for atomic layer growth *J. Phys. Chem.* **100** 13121–31
[93] Behera P S, Sarkar R and Bhattacharyya S 2009 Thin films: glassy alumina *NPG Asia Mater.* **NA** 10–6
[94] Pawłowski L 1988 The relationship between structure and dielectric properties in plasma-sprayed alumina coatings *Surf. Coat. Technol.* **35** 285–98
[95] Goswami A P, Roy S and Das G C 2002 Effect of powder, chemistry and morphology on the dielectric properties of liquid-phase-sintered alumina *Ceram. Int.* **28** 439–45

[96] Danks A E, Hall S R and Schnepp Z 2011 The evolution of 'sol-gel' chemistry as a technique for materials synthesis *Mater. Horiz.* **3** 91–112

[97] Park Y K, Tadd E H, Zubris M and Tannenbaum R 2005 Size-controlled synthesis of alumina nanoparticles from aluminum alkoxides *Mater. Res. Bull.* **40** 1506–12

[98] Nayar P, Waghmare S, Singh P, Najar M, Puttewar S and Agnihotri A 2020 Comparative study of phase transformation of Al_2O_3 nanoparticles prepared by chemical precipitation and sol–gel auto combustion methods *Mater. Today Proc.* **26** 122–5

[99] Sharma A, Rani A, Singh A, Modi O P and Gupta G K 2014 Synthesis of alumina powder by the urea–glycine–nitrate combustion process: a mixed fuel approach to nanoscale metal oxides *Appl. Nanosci.* **4** 315–23

[100] Huang KI, Yin LG, Liu SQ and Li CJ 2006 Preparation and formation mechanism of Al2O3 nanoparticles by reverse microemulsion *Trans. Nonferr. Met. Soc. China* **2007** 633–7

[101] Li J, Pan Y, Xiang C, Ge Q and Guo J 2006 Low temperature synthesis of ultrafine a -Al_2O_3 powder by a simple aqueous sol–gel process *Ceram. Int.* **32** 587–91

[102] Su X, Chen S and Zhou Z 2012 Applied surface science synthesis and characterization of monodisperse porous, -Al_2O_3 nanoparticles *Appl. Surf. Sci.* **258** 5712–5

[103] Laishram K, Mann R and Malhan N 2012 Short communication a novel microwave combustion approach for single step synthesis of a -Al_2O_3 nanopowders *Ceram. Int.* **38** 1703–6

[104] Boumaza A, Favaro L, Lédion J, Sattonnay G, Brubach J B, Berthet P, Huntz A M, Roy P and Tétot R 2009 Transition alumina phases induced by heat treatment of boehmite: an x-ray diffraction and infrared spectroscopy study *J. Solid State Chem.* **182** 1171–6

[105] Navrotsky A 2003 Energetics of nanoparticle oxides: interplay between surface energy and polymorphism† *Geochem. Trans.* **4** 34

[106] Huang X, Jiang P and Tanaka T 2011 A review of dielectric polymer composites with high thermal conductivity *IEEE Electr. Insul. Mag.* **27** 8–16

[107] Raju G G 2003 Appendix 3: selected properties of insulating materials *Dielectrics in Electric Fields* (New York: Dekker) pp 561–6

[108] Yu J, Huo R, Wu C, Wu X, Wang G and Jiang P 2012 Influence of interface structure on dielectric properties of epoxy/alumina nanocomposites *Macromol. Res.* **20** 816–26

[109] Crippa M, Bianchi A, Cristofori D, D'Arienzo M, Merletti F, Morazzoni F, Scotti R and Simonutti R 2013 High dielectric constant rutile-polystyrene composite with enhanced percolative threshold *J. Mater. Chem.* C **1** 484–92

[110] Lew C M, Sun M, Liu Y, Wang J and Yan Y 2009 Pure-silica-zeolite low-dielectric constant materials *Ordered Porous Solids* ed V Valtchev, S Mintova and M Tsapatsis (Amsterdam: Elsevier Science) pp 335–64

[111] Brunauer S, Kantro D L and Weise C H 1956 The surface energies of amorphous silica and hydrous amorphous silica *Can. J. Chem.* **34** 1483–96

[112] Hu W, Li L, Li G, Tang C and Sun L 2009 High-quality brookite TiO_2 flowers: synthesis, characterization, and dielectric performance *Cryst. Growth Des.* **9** 3676–82

[113] Yoko A, Umezawa N, Ohno T and Oshima Y 2018 Impact of surface energy on the formation of composite metal oxide nanoparticles *J. Phys. Chem.* C **122** 24350–8

[114] Babanzadeh S, Mehdipour-Ataei S and Mahjoub A R 2013 Effect of nanosilica on the dielectric properties and thermal stability of polyimide/SiO 2 nanohybrid *Des. Monomers Polym.* **16** 417–24

[115] Schmidt H 1994 Inorganic-organic composites by sol–gel techniques *J. Sol-gel Sci. Technol.* **1** 217–31

[116] Pujari S P, Scheres L, Marcelis A T M and Zuilhof H 2014 Covalent surface modification of oxide surfaces *Angew. Chem., Int. Ed.* **53** 6322–56

[117] Song Y, Shen Y, Liu H, Lin Y, Li M and Nan C-W 2012 Enhanced dielectric and ferroelectric properties induced by dopamine-modified $BaTiO_3$ nanofibers in flexible poly (vinylidene fluoride-trifluoroethylene) nanocomposites *J. Mater. Chem.* **22** 8063

[118] Luo H, Chen C, Zhou K, Zhou X, Wu Z and Zhang D 2015 Enhancement of dielectric properties and energy storage density in poly(vinylidene fluoride-co-hexafluoropropylene) by relaxor ferroelectric ceramics *RSC Adv.* **5** 68515–22

[119] Dang Z-M, Wang H-Y and Xu H-P 2006 Influence of silane coupling agent on morphology and dielectric property in $BaTiO_3$/polyvinylidene fluoride composites *Appl. Phys. Lett.* **89** 112902

[120] Kim P, Doss N M, Tillotson J P, Hotchkiss P J, Pan M-J, Marder S R, Li J, Calame J P and Perry J W 2009 High energy density nanocomposites based on surface-modified $BaTiO_3$ and a FERROELECTRIC POLymer *ACS Nano* **3** 2581–92

[121] Claude J, Lu Y, Li K and Wang Q 2008 Electrical storage in Poly(vinylidene fluoride) based Ferroelectric polymers: correlating polymer structure to electrical breakdown strength *Chem. Mater.* **20** 2078–80

[122] Jiang C, Zhang D, Zhou K, Zhou X, Luo H and Abrahams I 2016 Significantly enhanced energy storage density of sandwich-structured $(Na_{0.5}Bi_{0.5})_{0.93}Ba_{0.07}TiO_3$/P(VDF–HFP) composites induced by PVP-modified two-dimensional platelets *J. Mater. Chem.* A **4** 18050–9

[123] Zhang D, Wu Z, Zhou X, Wei A, Chen C and Luo H 2017 High energy density in P(VDF-HFP) nanocomposite with paraffin engineered $BaTiO_3$ nanoparticles *Sensors Actuators* A **260** 228–35

[124] Chang S-J, Liao W-S, Ciou C-J, Lee J-T and Li C-C 2009 An efficient approach to derive hydroxyl groups on the surface of barium titanate nanoparticles to improve its chemical modification ability *J. Colloid Interface Sci.* **329** 300–5

[125] Choudhury A 2012 Preparation, characterization and dielectric properties of polyetherimide nanocomposites containing surface-functionalized $BaTiO_3$ nanoparticles *Polym. Int.* **61** 696–702

[126] Zhou T, Zha J W, Cui R Y, Fan B H, Yuan J K and Dang Z M 2011 Improving dielectric properties of $BaTiO_3$/ferroelectric polymer composites by employing surface hydroxylated BaTiO3 nanoparticles *ACS Appl. Mater. Interfaces* **3** 2184–8

[127] Yang X, Jiang Z, Li W, Wang C, Chen M and Zhang G 2020 The role of interfacial H-binding in electric properties of UV-cured resin filled with hydroxylated Al_2O_3 nanopaticles *Nanotechnology* **31** 275710

[128] Allen A O, Hochanadel C J, Ghormley J A and Davis T W 1952 Decomposition of water and aqueous solutions under mixed fast neutron and γ-radiation *J. Phys. Chem.* **56** 575–86

[129] Lin Y-J and Hung C-C 2018 Temperature-dependent field-effect carrier mobility in organic thin-film transistors with a gate SiO_2 dielectric modified by H_2O_2 treatment *Appl. Phys.* A **124** 173

[130] Ashley K M, Carson Meredith J, Amis E, Raghavan D and Karim A 2003 Combinatorial investigation of dewetting: polystyrene thin films on gradient hydrophilic surfaces *Polymer* **44** 769–72

[131] Bai Y, Liu X, Chen L, Khizar-ul-Haq, Khan M A, Zhu W Q, Jiang X Y and Zhang Z L 2007 Organic thin-film field-effect transistors with MoO_3/Al electrode and OTS/SiO_2 bilayer gate insulator *Microelectron. J.* **38** 1185–90

[132] Dong B X, Amonoo J A, Purdum G E, Loo Y-L and Green P F 2016 Enhancing carrier mobilities in organic thin-film transistors through morphological changes at the semiconductor/dielectric interface using supercritical carbon dioxide processing *ACS Appl. Mater. Interfaces* **8** 31144–53

[133] Li Q, Li S, Yang D, Su W, Wang Y, Zhou W, Liu H and Xie S 2017 Designing hybrid gate dielectric for fully printing high-performance carbon nanotube thin film transistors *Nanotechnology* **28** 0–31

[134] Saxena V, Chauhan A K, Padma N, Aswal D K, Koiry S P, Sen S, Tokas R B, Gupta S K, Sürgers C and Yakhmi J V 2009 Poly(3-hexylthiophene) based field-effect transistors with gate SiO_2 dielectric modified by multi-layers of 3-aminopropyltrimethoxysilane *Thin Solid Films* **517** 6124–8

[135] Cao L, Peng Y and Li Z 2016 Phosphonic acid self-assembled monolayer improved the properties of n-type organic field-effect transistors in air ambient *RSC Adv.* **6** 89794–8

[136] Ismail A G and Hill I G 2011 Stability of n-channel organic thin-film transistors using oxide, SAM-modified oxide and polymeric gate dielectrics *Org. Electron.* **12** 1033–42

[137] Majewski L A, Schroeder R and Grell M 2005 Low-voltage, high-performance organic field-effect transistors with an ultra-thin TiO_2 layer as gate insulator *Adv. Funct. Mater.* **15** 1017–22

[138] Kim S, Ha T, Yoo S, Ka J W, Kim J, Won J C, Choi D H, Jang K S and Kim Y H 2017 Metal-oxide assisted surface treatment of polyimide gate insulators for high-performance organic thin-film transistors *Phys. Chem. Chem. Phys.* **19** 15521–9

[139] Yuan Y, Lin H, Yu D, Yin Y, Tang B, Li E and Zhang S 2017 Effects of perfluorooctyltriethoxysilane coupling agent on the properties of silica filled PTFE composites *J. Mater. Sci.: Mater. Electron.* **28** 8810–7

[140] Adnan M M, Tveten E G, Miranti R, Hvidsten S, Ese M H G, Glaum J and Einarsrud M A 2020 *In situ* synthesis of epoxy nanocomposites with hierarchical surface-modified SiO_2 clusters *J. Sol-Gel Sci. Technol.* **95** 783–94

[141] Chi Q, Wang B, Zhang T, Zhang C, Zhang Y, Wang X and Lei Q 2019 Designing of surface modification and sandwich structure: effective routs to improve energy storage property in polyimide-based composite films *J. Mater. Sci.: Mater. Electron.* **30** 19956–65

[142] Yang H, Gao Q, Xie Y, Chen Q, Ouyang C, Xu Y and Ji X 2015 Effect of SiO_2 and TiO_2 nanoparticle on the properties of phenyl silicone rubber *J. Appl. Polym. Sci.* **132** 1–9

[143] Dang Z M, Xia Y J, Zha J W, Yuan J K and Bai J 2011 Preparation and dielectric properties of surface modified TiO_2/silicone rubber nanocomposites *Mater. Lett.* **65** 3430–2

[144] Wang W and Li S 2019 Improvement of dielectric breakdown performance by surface modification in polyethylene/TiO_2 nanocomposites *Materials* **12** 3346

[145] Khodaparast P and Ounaies Z 2013 On the impact of functionalization and thermal treatment on dielectric behavior of low content TiO_2 PVDF nanocomposites *IEEE Trans. Dielectr. Electr. Insul.* **20** 166–76

[146] Fan Y, Wang G, Huang X, Bu J, Sun X and Jiang P 2016 Molecular structures of (3-aminopropyl)trialkoxysilane on hydroxylated barium titanate nanoparticle surfaces induced by different solvents and their effect on electrical properties of barium titanate based polymer nanocomposites *Appl. Surf. Sci.* **364** 798–807

[147] Dalle Vacche S, Oliveira F, Leterrier Y, Michaud V, Damjanovic D and Månson J A E 2014 Effect of silane coupling agent on the morphology, structure, and properties of poly(vinylidene fluoride-trifluoroethylene)/$BaTiO_3$ composites *J. Mater. Sci.* **49** 4552–64

[148] Gu L, Li T, Xu Y, Sun C, Yang Z, Zhu D and Chen D 2019 Effects of the particle size of $BaTiO_3$ fillers on fabrication and dielectric properties of $BaTiO_3$/Polymer/Al films for capacitor energy-storage application *Materials* **12** 439

[149] Iijima M, Sato N, Wuled Lenggoro I and Kamiya H 2009 Surface modification of BaTiO3 particles by silane coupling agents in different solvents and their effect on dielectric properties of $BaTiO_3$/epoxy composites *Colloids Surf.* A **352** 88–93

[150] Dang Z M, Yu Y F, Xu H P and Bai J 2008 Study on microstructure and dielectric property of the $BaTiO_3$/epoxy resin composites *Compos. Sci. Technol.* **68** 171–7

[151] Huang X, Xie L, Jiang P, Wang G and Liu F 2009 Electrical, thermophysical and micromechanical properties of ethylene-vinyl acetate elastomer composites with surface modified $BaTiO_3$ nanoparticles *J. Phys. D: Appl. Phys.* **42** 245407

[152] Chao F and Liang G 2009 Effects of coupling agent on the preparation and dielectric properties of novel polymer-ceramic composites for embedded passive applications *J. Mater. Sci.: Mater. Electron.* **20** 560–4

[153] Wenying Z and Demei Y 2011 Effect of coupling agents on the dielectric properties of aluminum particles reinforced epoxy resin composites *J. Compos. Mater.* **45** 1981–9

[154] Cheng Q, Li C, Pavlinek V, Saha P and Wang H 2006 Surface-modified antibacterial TiO_2/Ag^+ nanoparticles: preparation and properties *Appl. Surf. Sci.* **252** 4154–60

[155] Ma D, Hugener T A, Siegel R W, Christerson A, Mårtensson E, Önneby C and Schadler L S 2005 Influence of nanoparticle surface modification on the electrical behaviour of polyethylene nanocomposites *Nanotechnology* **16** 724–31

[156] Karlsson M 2014 *Investigation of the Dielectric Breakdown Strength of Polymer Nanocomposites* Uppasala University, Uppsala, Sweden *Master's Thesis*, UPTEC Q14 009 (accessed: 7 July, 2020) (https://www.diva-portal.org/smash/get/diva2:731544/FULLTEXT01.pdf)

[157] Chiang C H, Ishida H and Koenig J L 1980 The structure of γ-aminopropyltriethoxysilane on glass surfaces *J. Colloid Interface Sci.* **74** 396–404

[158] Chao F, Liang G, Kong W and Zhang X 2008 Study of dielectric property on $BaTiO_3$/BADCy composite *Mater. Chem. Phys.* **108** 306–11

[159] Costes M, Naulin C, Dorthe G, Vaucamps C and Nouchi G 1987 Dynamics of the reactions of aluminium atoms studied with pulsed crossed supersonic molecular beams *Faraday Discuss. Chem. Soc.,* **84** 75–86

[160] Neouze MA and Schubert U 2008 Review surface modification and functionalization of metal and metal oxide nanoparticles by organic ligands *Monatsh Chem* **139** 183–95

[161] Wåhlander M, Nilsson F, Larsson E, Tsai W C, Hillborg H, Carlmark A, Gedde U W and Malmström E 2014 Polymer-grafted Al2O3-nanoparticles for controlled dispersion in poly(ethylene-co-butyl acrylate) nanocomposites *Polymer* **55** 2125–38

[162] Cobo Sánchez C, Wåhlander M, Taylor N, Fogelström L and Malmström E 2015 Novel nanocomposites of Poly(lauryl methacrylate)-Grafted Al_2O_3 nanoparticles in LDPE *ACS Appl. Mater. Interfaces* **7** 25669–78

[163] Gong Y *et al* 2019 Core–shell structured Al/PVDF nanocomposites with high dielectric permittivity but low loss and enhanced thermal conductivity *Polym. Eng. Sci.* **59** 103–11

[164] Acton O, Ting G G, Shamberger P J, Ohuchi F S, Ma H and Jen A K Y 2010 Dielectric surface-controlled low-voltage organic transistors via n-alkyl phosphonic acid self-assembled monolayers on high-k metal oxide *ACS Appl. Mater. Interfaces* **2** 511–20

[165] Hanson E L, Schwartz J, Nickel B, Koch N and Danisman M F 2003 Bonding self-assembled, compact organophosphonate monolayers to the native oxide surface of silicon *J. Am. Chem. Soc.* **125** 16074–80

[166] Hotchkiss P J, Jones S C, Paniagua S A, Sharma A, Kippelen B, Armstrong N R and Marder S R 2012 The modification of indium tin oxide with phosphonic acids: mechanism of binding, tuning of surface properties, and potential for use in organic electronic applications *Acc. Chem. Res.* **45** 337–46

[167] Li Z and Luo X 2014 ADO-phosphonic acid self-assembled monolayer modified dielectrics for organic thin film transistors *J. Semicond.* **35** 104004

[168] Chen X, Liang F, Lu W, Jin Z, Zhao Y and Fu M 2018 High permittivity nanocomposites embedded with Ag/TiO_2 core–shell nanoparticles modified by phosphonic acid *Polymers* **10** 586

[169] Chen X, Liang F, Lu W, Zhao Y, Fan G and Wang X 2018 Improved dielectric properties of Ag@TiO2/PVDF nanocomposites induced by interfacial polarization and modifiers with different carbon chain lengths *Appl. Phys. Lett.* **112** 1–6

[170] Siddabattuni S, Schuman T P and Dogan F 2013 Dielectric properties of polymer-particle nanocomposites influenced by electronic nature of filler surfaces *ACS Appl. Mater. Interfaces* **5** 1917–27

[171] Ehrhardt C *et al* 2013 $BaTiO_3$-P(VDF-HFP) nanocomposite dielectrics—influence of surface modification and dispersion additives *Mater. Sci. Eng.* B **178** 881–8

[172] Kim P, Jones S C, Hotchkiss P J, Haddock J N, Kippelen B, Marder S R and Perry J W 2007 Phosphonic acid-modified barium titanate polymer nanocomposites with high permittivity and dielectric strength *Adv. Mater.* **19** 1001–5

[173] Ye H J, Shao W Z and Zhen L 2013 Tetradecylphosphonic acid modified $BaTiO_3$ nanoparticles and its nanocomposite *Colloids Surf.* A **427** 19–25

[174] Ehrhardt C, Fettkenhauer C, Glenneberg J, Münchgesang W, Leipner H S, Wagner G, Diestelhorst M, Pientschke C, Beige H and Ebbinghaus S G 2014 Enhanced dielectric properties of sol-gel-$BaTiO_3$/P(VDF-HFP) composite films without surface functionalization *RSC Adv.* **4** 40321–9

[175] Lee H, Dellatore S M, Miller W M and Messersmith P B 2007 Mussel-inspired surface chemistry for multifunctional coatings *Science* **318** 426–30

[176] Shultz M D, Reveles J U, Khanna S N and Carpenter E E 2007 Reactive nature of dopamine as a surface functionalization agent in iron oxide nanoparticles *J. Am. Chem. Soc.* **129** 2482–7

[177] Liao S, Shen Z, Pan H, Zhang X, Shen Y, Lin Y H and Nan C W 2017 A surface-modified TiO_2 nanorod array/P (VDF-HFP) dielectric capacitor with ultra high energy density and efficiency *J. Mater. Chem.* C **5** 12777–84

[178] Huang Q, Luo H, Chen C, Zhou K and Zhang D 2018 Improved energy density and dielectric properties of P(VDF-HFP) composites with TiO_2 nanowire clusters *J. Electroceramics* **40** 65–71

[179] Wang G, Huang X and Jiang P 2017 Bio-inspired polydopamine coating as a facile approach to constructing polymer nanocomposites for energy storage *J. Mater. Chem.* C **5** 3112–20

[180] Wang L, Luo H, Zhou X, Wei A, Zhou K, Chen Z and Zhang D 2018 Enhanced permittivity and energy density of P(VDF-HFP)-based capacitor using core–shell structured $BaTiO_3$@TiO_2 fillers *Ionics* **24** 3975–82

[181] Yang D, Ruan M, Huang S, Wu Y, Li S, Wang H, Shang Y, Li B, Guo W and Zhang L 2016 Improved electromechanical properties of NBR dielectric composites by poly(dopamine) and silane surface functionalized TiO_2 nanoparticles *J. Mater. Chem.* C **4** 7724–34

[182] Pan Z, Yao L, Zhai J, Shen B and Wang H 2017 Significantly improved dielectric properties and energy density of polymer nanocomposites via small loaded of $BaTiO_3$ nanotubes *Compos. Sci. Technol.* **147** 30–8

[183] Nie X, Zhu K, Sun Q, Liu J, Wang J, Yan K and Zeng K 2018 Enhanced discharged energy density of nanocomposites with dopamine@$BaTiO_3$ whiskers *Mater. Technol.* **00** 1–7

[184] Xie B, Zhang Q, Zhang H, Zhang G, Qiu S and Jiang S 2016 Largely enhanced ferroelectric and energy storage performances of P(VDF-CTFE) nanocomposites at a lower electric field using $BaTiO_3$ nanowires by stirring hydrothermal method *Ceram. Int.* **42** 19012–8

[185] Luo B, Wang X, Zhao Q and Li L 2015 Synthesis, characterization and dielectric properties of surface functionalized ferroelectric ceramic/epoxy resin composites with high dielectric permittivity *Compos. Sci. Technol.* **112** 1–7

[186] Wu M, Yuan X, Luo H, Chen H, Chen C, Zhou K and Zhang D 2017 Enhanced actuation performance of piezoelectric fiber composites induced by incorporated $BaTiO_3$ nanoparticles in epoxy resin *Phys. Lett.* A **381** 1641–7

[187] Zhan Y, Zhang J, He S, Zhao S, Bai Y and Liu X 2019 Thermally stable and dielectric nanocomposite based on poly(arylene ether nitrile) and $BaTiO_3$ functionalized by modified mussel-inspired route *J. Polym. Res.* **26** 77

[188] Ruan M, Yang D, Guo W, Zhang L, Li S, Shang Y, Wu Y, Zhang M and Wang H 2018 Improved dielectric properties, mechanical properties, and thermal conductivity properties of polymer composites via controlling interfacial compatibility with bio-inspired method *Appl. Surf. Sci.* **439** 186–95

[189] Yang D, Huang S, Ruan M, Li S, Yang J, Wu Y, Guo W and Zhang L 2018 Mussel inspired modification for aluminum oxide/silicone elastomer composites with largely improved thermal conductivity and low dielectric constant *Ind. Eng. Chem. Res.* **57** 3255–62

[190] Duan G, Cao Y, Quan J, Hu Z, Wang Y, Yu J and Zhu J 2020 Bioinspired construction of BN@polydopamine@Al_2O_3 fillers for preparation of a polyimide dielectric composite with enhanced thermal conductivity and breakdown strength *J. Mater. Sci.* **55** 8170–84

[191] Xie L, Huang X, Huang Y, Yang K and Jiang P 2013 Core@Double-shell structured $BaTiO_3$-polymer nanocomposites with high dielectric constant and low dielectric loss for energy storage application *J. Phys. Chem.* C **117** 22525–37

[192] Li H Z, Li W Z, Yang Y J, Tai H L, Du X S, Gao R Y and Li S Y 2018 Pyroelectric performances of 1-3 ferroelectric composites based on barium titanate nanowires/ polyvinylidene fluoride *Ceram. Int.* **44** 19254–61

[193] López Zavala M Á, Lozano Morales S A and Ávila-Santos M 2017 Synthesis of stable TiO_2 nanotubes: effect of hydrothermal treatment, acid washing and annealing temperature *Heliyon* **3** e00456